無電鍍沉積二氧化釕與釕複合薄膜之特性研究

學生：陳境妤　　　　　　　　　　　　　　　　指導教授：吳樸偉 博士

國立交通大學材料科學與工程學系

摘要

35–300 nm 非晶形二氧化釕及釕之複合薄膜已成功地以一新開發的鍍液配方，用無電鍍沉積的方式沉積在銅基板上。其無電鍍液之成份為：$K_2RuCl_5 \cdot xH_2O$、$NaNO_2$、NaOH、NaClO。不同鍍液製備步驟、三種不同濃度之 $NaNO_2$、及不同沉積時間為本研究之操作變因。本研究討論其反應方程式來說明無電鍍液之沉積機制。紫外光-可見光光譜圖之最大吸收波長的窄小分佈，顯示無電鍍液之穩定程度。此外，利用能量散佈光譜儀、掃描式電子顯微鏡、原子力顯微鏡、X 光光電子譜儀、拉曼散射光譜儀來研究二氧化釕與釕複合薄膜之特性。結果顯示，以 0.06 M $NaNO_{2(aq)}$為配方之無電鍍液為最佳之參數。另外，藉由 2 小時氫氣還原在 200℃下還原其複合薄膜，可得到結晶之金屬釕薄膜。而非晶形之複合薄膜，在 2 小時的氬氣高溫退火 400℃的環境下可得結晶之二氧化釕與釕之複合薄膜。

Electroless Deposition of Composite Ruthenium Oxide and Ruthenium Films

Student: Jing-Yu Chen　　　　　　Advisor: Dr. Pu-Wei Wu

Department of Materials Science and Engineering

National Chiao Tung University

Abstract

A 35–300 nm amorphous ruthenium oxide and ruthenium composite film has been deposited by electroless plating on a Cu substrate. The plating solution contained compounds of $K_2RuCl_5 \cdot xH_2O$, $NaNO_2$, NaOH, and NaClO. Variables including different mixing steps, concentrations of $NaNO_{2(aq)}$, and plating time were investigated. The reaction steps for the electroless plating were indentified. Stability of the plating solution was confirmed by UV-Vis absorption spectra with narrow maximum wavelength distribution. EDX, SEM, AFM, XPS, and Raman spectroscopy were employed to characterize the as-deposited films. It was concluded that the plating solution with 0.06 M $NaNO_{2(aq)}$ delivered the desirable film qualities. A crystalline Ru film was obtained by H_2 reduction for the as-deposited film at 200℃ for 2 hr. In addition, we were able to produce a crystalline RuO_2 and Ru composite film by Ar annealing of the as-deposited film at 400℃ for 2 hr.

Acknowledgements

To begin with, I would express my appreciation to Department of Materials Science and Engineering, Library, and Center for Nanoscience and Technology in National Chiao Tung University.

Second, I would like thank my advisor, Prof. Pu-Wei Wu. Because of his guidance and suggestions during my M.S. research, I could finish this study. Besides, I would like express my appreciation to my oral committees, Prof. Fu-Ming Pan and Prof. Fu-Hsiang Ko.

Third, I am much obliged to my co-workers and those who have helped me. I am thankful for Rachel's experience in Ru electroless plating, Lawrence's help for EDX measurement, and Robert's assistance for XPS detection. In addition, I would like thank Yunmin's discussion for drawing figures and Evan's favor for Ar annealing. Furthermore, I acknowledge to Matt's favor for AFM measurement, Hedy's assistance for UV-Vis spectra recording, and Alan's discussion for stress.

On the other hand, I would also like to express my appreciation to my friends, Frida, Fanny, and Monica. Because of their kindness and interesting personality, I can get enjoyment from my leisure time.

最後我要感謝我的父母和家人對我的支持與鼓勵。謝謝我的父親陳靖田先生與我的母親王麗霞女士，感謝他們對我在教育上的栽培與精神上的鼓勵，使我能專心於學業而無後顧之憂。

Contents

摘要 .... **i**

Abstract .... **ii**

Acknowledgements .... **iii**

Contents .... **iv**

List of Tables .... **vii**

List of Figures .... **viii**

Chapter 1 Introduction **1**

Chapter 2 Literature Review **4**

2.1 Physical and chemical properties of RuO_2 and Ru 4

2.2 Applications of RuO_2 films 5

2.3 Fabrications of RuO_2 films 5

2.3.1 Vacuum deposition *5*

2.3.2 Solution deposition *7*

2.3.3 Other methods *7*

2.4 Applications of Ru films 8

2.5 Fabrications of Ru films 8

2.5.1 Vacuum deposition *8*

2.5.2 Solution deposition *10*

Chapter 3 Experimental **16**

3.1 Experimental design 16

3.2 Materials 17

3.3 Plating bath preparation 17

3.4 Instruments and characterization 20

Chapter 4 Results and Discussion I: Development of Ru electroless plating solution 22

4.1 Development of plating bath components.. 22

4.2 Deposition mechanism 24

4.3 Stability of plating solution 25

Chapter 5 Results and Discussion II: Characterization of composite RuO_2 and Ru films 30

5.1 Characterization of composite RuO_2 and Ru films 30

5.1.1 The existence of Ru element in the deposited films *30*

5.1.2 Morphology observation and thickness measurement of the deposited films *32*

5.1.3 Thickness at different plating time *38*

5.1.4 Roughness measurement for the deposited films *39*

5.1.5 Characterization of the oxidation states for the deposited films *41*

5.1.6 Phase and crystallinity characterization for the deposited films *47*

5.1.7 Raman spectroscopy characterization for the deposited films *48*

5.2 Characterization of the composite RuO_2 and Ru films after hydrogen reduction 52

5.2.1 Morphology observation of the deposited films after hydrogen reduction. *52*

5.2.2 Phase and crystallinity characterization for the deposited films after hydrogen reduction *56*

5.2.3 Characterization of the oxidation states for the deposited films after

hydrogen reduction *58*

5.2.4 Raman spectroscopy characterization for the deposited films after hydrogen reduction *60*

5.3 Characterization of composite RuO_2 and Ru films after argon annealing 63

5.3.1 Morphology observation of the deposited films after argon annealing *63*

5.3.2 Phase and crystallinity characterization for the deposited films after argon annealing *65*

Chapter 6 Conclusions **67**

References **69**

List of Tables

Table 2.1 Physical and chemical properties of RuO_2 and Ru. 4

Table 2.2 Components of the electroless Ru plating bath A [15]. 13

Table 2.3 Components of the electroless Ru plating bath B [18]. 14

Table 2.4 Components of the electroless Ru plating bath C [16]. 14

Table 2.5 Components of the electroless Ru plating bath D [9, 17]. 15

Table 3.1 Materials used in this research. 17

Table 4.1 The distribution of the maximum absorption wavelength between 300 nm and 500 nm. 29

Table 5.1 R_q of the deposited films under selective plating time in different concentrations of $NaNO_{2(aq)}$. 39

Table 5.2 Relative amounts of Ru in different forms from XPS spectra from Figure 5.10 to Figure 5.12. 46

List of Figures

Figure 3.1 Experimental flowchart. 16

Figure 3.2 Structures of the substrate for electroless plating. 18

Figure 3.3 The adding steps of the plating bath. 19

Figure 4.1 Four different adding steps for the plating bath...................................... 23

Figure 4.3 Evolution of the absorbance from the maximum absorption wavelength of UV-Vis spectra in various time under different temperatures; (a) at 40℃, and (b) at room temperature.. 28

Figure 5.1 EDX results from the deposited films with 0.06 M $NaNO_{2(aq)}$ at various plating time; (a) 30, (b) 60, and (c) 240 min, respectively. (d)–(f) were the corresponding spectrum. 31

Figure 5.2 Planar views for the deposited films at various plating time with 0.6 M $NaNO_{2(aq)}$; (a) 30, (b) 60, (c) 120, (d) 240, and (e) 480 min, respectively. 34

Figure 5.3 Planar views for the deposited films at various plating time with 0.06 M $NaNO_{2(aq)}$; (a) 30, (b) 60, (c) 120, (d) 240, and (e) 480 min, respectively. 35

Figure 5.4 Planar views for the deposited films at various plating time with 0.03 M $NaNO_{2(aq)}$; (a) 30, (b) 60, (c) 120, (d) 240, and (e) 480 min, respectively. 36

Figure 5.5 Cross-sectional views for the deposited films at various plating time with 0.06 M $NaNO_{2(aq)}$; (a) 30, (b) 60, (c) 120, (d) 240, and (e) 480 min, respectively; and (f) the smaller scope of (e)...................................... 37

Figure 5.6 Thicknesses for the deposited films versus various plating time with different concentrations of $NaNO_{2(aq)}$.. 38

Figure 5.7 Roughness of the deposited films at three different concentrations of $NaNO_{2(aq)}$ in various plating time; (a)–(c) are at 10 min, and (d)–(f) are at 120 min; (a) 0.6, (b) 0.06, (c) 0.03, (d) 0.6, (e) 0.06, and (f) 0.03 M $NaNO_{2(aq)}$. 40

Figure 5.8 XPS spectra for the Ru 3p3/2 line from the deposited films with 0.06 M $NaNO_{2(aq)}$ at various plating time; (a) 30, (b) 120, and (c) 480 min, respectively. 44

Figure 5.9 XPS spectra for the O 1s line from the deposited films with 0.06 M $NaNO_{2(aq)}$ at various plating times, (a) 30, (b) 120, and (c) 480 min, respectively. 44

Figure 5.10 XPS spectra for the Ru 3p3/2 line including both experimental and curve fitting of the deposited film with 0.6 M $NaNO_{2(aq)}$ for 30 min plating time.. 45

Figure 5.11 XPS spectra for the Ru 3p3/2 line including both experimental and curve fitting of the deposited film with 0.06 M $NaNO_{2(aq)}$ for 30 min plating time.. 45

Figure 5.12 XPS spectra for the Ru 3p3/2 line including both experimental and curve

fitting of the deposited film with 0.03 M $NaNO_{2(aq)}$ for 30 min plating time. 46

Figure 5.13 XRD patterns for the as-deposited films with various concentrations of NaNO2(aq) for 480 min plating time versus the standard pattern; (a) 0.03 (b) 0.06, and (c) 0.6 M, respectively. 48

Figure 5.14 Raman spectra for the composite films with 0.6 M $NaNO_{2(aq)}$ at various plating time; (a) Cu substrate as a blank, (b) 30, (c) 60, (d) 120, (e) 240, and (f) 480 min, respectively. 50

Figure 5.15 Raman spectra for the composite films with 0.06 M $NaNO_{2(aq)}$ at various plating time; (a) Cu substrate as a blank, (b) 30, (c) 60, (d) 120, (e) 240, and (f) 480 min, respectively. 50

Figure 5.16 Raman spectra of the composite films with 0.03 M $NaNO_{2(aq)}$ at various plating time; (a) Cu substrate as a blank, (b) 30, (c) 60, (d) 120, (e) 240, and (f) 480 min, respectively. 51

Figure 5.17 Planar views for the deposited films at various plating time with 0.6 M $NaNO_{2(aq)}$ after H_2 reduction at 200℃ for 2 hr; (a) 30, (b) 60, (c) 120, (d) 240, and (e) 480 min, respectively. 53

Figure 5.18 Planar views for the deposited films at various plating time with 0.06 M $NaNO_{2(aq)}$ after H_2 reduction at 200℃ for 2 hr; (a) 30, (b) 60, (c) 120, (d) 240, and (e) 480 min, respectively. 54

Figure 5.19 The planar views of deposited films at various plating time with 0.03 M $NaNO_{2(aq)}$ after H_2 reduction at 200℃ for 2 hr; (a) 30, (b) 60, (c) 120, (d)

240, and (e) 480 min, respectively. 55

Figure 5.20 XRD patterns for the as-deposited films with various concentrations $NaNO_{2(aq)}$ for 480 min plating time and followed by H_2 reduction at 200 ℃ for 2 hr versus the standard pattern; (a) 0.03, (b) 0.06, and (c) 0.6 M, respectively. 57

Figure 5.21 XPS spectra for the Ru 3p3/2 line from the deposited films with 0.06 M $NaNO_{2(aq)}$ at various plating time followed by H_2 reduction at 200℃ for 2 hr; (a) 120 and (b) 480 min, respectively... 59

Figure 5.22 XPS spectra for the O 1s line from the deposited films with 0.06 M $NaNO_{2(aq)}$ at various plating time followed by H_2 reduction at 200℃ for 2 hr; (a) 120 and (b) 480 min, respectively... 59

Figure 5.23 Raman spectra for the composite films with 0.6 M $NaNO_{2(aq)}$ at various plating times after H_2 reduction; (a) Cu substrate as a blank, (b) 30, (c) 60, (d) 120, (e) 240, and (f) 480 min, respectively............................... 61

Figure 5.24 Raman spectra for the composite films with 0.06 M $NaNO_{2(aq)}$ at various plating times after H_2 reduction; (a) Cu substrate as a blank, (b) 30, (c) 60 , (d) 120, (e) 240, and (f) 480 min, respectively............................. 61

Figure 5.25 Raman spectra for the composite films with 0.03 M $NaNO_{2(aq)}$ at various plating times after H_2 reduction; (a) Cu substrate as a blank, (b) 30, (c) 60, (d) 120, (e) 240, and (f) 480 min, respectively............................... 62

Figure 5.26 Planar views for the deposited films at various plating time with 0.06 M $NaNO_{2(aq)}$ followed by Ar annealing at 400℃ for 2 hr; (a) 30, (b) 120,

and (c) 480 min, respectively. 64

Figure 5.27 XRD patterns for the as-deposited films with various concentrations $NaNO_{2(aq)}$ for 480 min plating time followed by Ar annealing at 400℃ for 2 hr versus the standard pattern; (a) 0.03, (b) 0.06, and (c) 0.6 M, respectively. 66

Chapter 1 Introduction

Ruthenium, as one of the platinum groups metals (PGMs), is a relatively inexpensive element compared with others in PGMs. In addition, because of its unique physical and chemical properties, such as low resistivity and excellent chemical stability, ruthenium has attracted considerable interests as electrocatalysts [1] or diffusion barriers [2-6]. In addition, ruthenium oxide (RuO_2), the most stable oxide form of ruthenium, demonstrates high conductivity and excellent electrochemical reversibility. Therefore, in recent years, researchers have become increasingly devoted to the in deposition of ruthenium oxide for supercapacitors application [7-14].

So far, many deposition methods for ruthenium and ruthenium oxide thin films have been developed. However, as technology requirements increase, so do demand for better films quality control. For example, films uniformity and step coverage are of particular concern. The fabrications of ruthenium and ruthenium oxide films can be divided into two categories; vacuum deposition and solution deposition. Vacuum deposition can be subdivided into three fabrication routes; physical vapor deposition, chemical vapor deposition, and atomic layer deposition. On the other hand, solution deposition is mainly composed of electrodeposition and electroless deposition. However, thin films containing ruthenium deposited by vacuum deposition require low pressure equipment. Besides, excess waste from sputtering or evaporation is an unavoidable concern in thin films deposited by vacuum deposition. In contrast, solution deposition can be performed under atmospheric pressure with relatively low cost. Moreover, the area by solution route can be much larger than that by vacuum deposition.

Electroless deposition, which is often called autocatalytic deposition, was first introduced by Brenner and Riddell in 1946. In comparison to electrodeposition, electroless deposition can be operated without an external current. In addition, many unique properties can be obtained via the electroless deposition as opposed to the electrodeposition. For example, electroless plating can deposit metals on subjects with sophisticated shapes and as well as high aspect-ratio holes. Deposits by autocatalytic deposition are typically denser and exhibits better properties for corrosion and electronics applications. Furthermore, electroless deposition is particularly suited to non-conductive surface and selective coverage on the catalyzed areas of the substrates.

In general, the composition in an electroless plating formulation consists of several components; metal ions, complexing agents, reducing agents, stabilizers, and inhibitors. Metal ions are provided by metal precursors. Complexing agents, stabilizers, and inhibitors are used to prepare an appropriate plating solution. In addition, reducing agents are employed to provide the necessary electron to reduce the metal ions during the autocatalytic deposition. It is to be noted that the selection of complexing agents and reducing agents depends on the condition of plating solution, such as pH value and metals to be deposited.

Owing to the pioneering contribution from Brenner and Riddell, the electroless nickel deposition has been the most well-established chemistry in electroless deposition. In addition to nickel, cobalt, copper, silver, gold, and palladium are also studied. The platinum group metals, whose positions are near these metals mentioned above in the periodic table, have been received significant attention by researchers in the past two decades in the field of electroless deposition. However, most publications

related the electroless plating of PGMs primarily focus on palladium and platinum. Other four metals in this group, ruthenium, osmium, rhodium, and iridium, have been less investigated.

Ruthenium is relatively inexpensive among PGMs compared with palladium, platinum, and other three metals in this group. However, because of its presence in multiple oxidation states and possible disproportionation reactions in solutions, electroless deposition of ruthenium metal is more difficult to achieve compared with platinum and palladium in PGMs.

To our best knowledge, only a few publications have documented in ruthenium electroless deposition [9, 15-18]. Despite that the specific qualitative characterizations were not mentioned in these investigations. The details for plating solution preparation and deposition mechanism of ruthenium were not be discussed carefully by the researchers. Therefore, the objective for this research is to develop a practical ruthenium electroless plating solution with a unique recipe corresponding mechanism properly explained. In addition, the properties of deposited films containing ruthenium are investigated.

Chapter 2 Literature Review

Many fabrication techniques for ruthenium oxide and ruthenium films have been developed. They can be mainly divided into two categories; vacuum deposition and solution deposition. Vacuum deposition includes physical vapor deposition (PVD), chemical vapor deposition (CVD), and atomic layer deposition (ALD). Solution deposition includes electrodeposition and electroless deposition.

2.1 Physical and chemical properties of RuO_2 and Ru

Table 2.1 Physical and chemical properties of RuO_2 and Ru.

Parameter	Ruthenium oxide [19]	Ruthenium [20]
Molecular or atomic weight	133.07	101.07
Crystal structure	rutile	hcp
Lattice constant	a = 4.491 Å c = 3.107 Å c/a = 0.691	a = 2.71 Å c = 4.28 Å c/a = 1.583
Color	Blue-black	White
Density (g/cm^3)	7.05	12.45
Electrical conductivity ($\Omega^{-1}cm^{-1}$)	$2\times10^4 - 3\times10^4$ (25℃)	$\sim1.4\times10^5$ (25℃)

2.2 Applications of RuO_2 films

The RuO_2 films can be used in Cu interconnection and capacitor electrodes [14]. The ruthenium oxide films are used in Cu interconnection because of its properties, such as low bulk resistivity, good thermal stability, and diffusion barrier capability. Furthermore, the RuO_2 films demonstrate some additional advantages like a wide potential window of reversible redox potentials, relatively high specific capacitance, and a very long cycle life. These attributes make them suitable capacitor electrodes [11]. Moreover, amorphous ruthenium oxide films have been widely used for supercapacitors owing to their high specific capacitance, high conductivity, and good electrochemical reversibility [8].

2.3 Fabrications of RuO_2 films

2.3.1 Vacuum deposition

Physical Vapor Deposition (PVD)

Ruthenium oxide films have been deposited by reactive sputtering [21] and r.f. magnetron sputtering [2] instead of dc sputtering. It is because the dc sputtering can only be used to deposit conductor. In addition to typical drawbacks of PVD such as low pressure deposition condition and unnecessary waste of target, the exact control of composition is another challenge for the PVD to deposit RuO_2 films.

Chemical Vapor Deposition (CVD)

Compared with RuO_2 films by the PVD, the RuO_2 films fabricated via the chemical vapor deposition (CVD) have many advantages, including low cost, easy compositions control, excellent step coverage, and compatibility to large-scaled processing [22]. Unfortunately, the deposition temperature in the CVD is relatively high. In 1993, Yuan *et al.* used RuO_4 as a precursor to deposit ruthenium oxide films by CVD [23]. At the same year, Si *et al.* reported $Ru(Cp)_2$ as a precursor to produce polycrystalline RuO_2 films by metal-organic chemical vapor deposition (MOCVD) on three different substrates [22]. Until recently, needle-like structures of ruthenium dioxide films have been deposited with ozone-mediated CVD by Hashaikeh *et al.* [24]. Ozone was used to produce mixture of $RuO_{4(g)}$, air, and $O_{3(g)}$ in that research. However, the coverage and roughness of the deposited films in that study need further improvement.

Atomic Layer Deposition (ALD)

The advantage of RuO_2 films by the atomic layer deposition is that ultra thin films can be deposited. In 2007, Jin-Hyock Kim *et al.* deposited ruthenium oxide films by a modified ALD with $Ru(EtCp)_2$ precursor [14]. In comparison to the conventional ALD for RuO_2 films, polycrystalline RuO_2 were deposited by this new technique instead of RuO_2 and Ru composite.

2.3.2 Solution deposition

Electrodeposition

In comparison to the fabrication methods mentioned above, the electrodeposition is a relatively simple, one-step, and cost-effective approach. Moreover, the electrodeposition provides advantages in preparation of uniform thin films for ruthenium oxide on substrates with complicated shapes and nanoporous structures. In 1999, Hu *et al.* used electrodeposition to deposit amorphous ruthenium oxide films on titanium substrates [7]. Later in 2007, the same group improved further using anodic deposition to produce amorphous ruthenium oxide films on identical substrates [13]. Similar work was done by Il-Hwan Kim *et al.*, where ruthenium oxide films on three different substrates were obtained by electrodeposition [12]. However, roughness and denseness of the deposited films in their study were not optimized yet.

2.3.3 Other methods

In addition to vacuum deposition and solution deposition, some other methods have been reported in RuO_2 films fabrication, such as organic precursor method [8], thermal decomposition [25], and electrostatic spray deposition [11]. In 2001, Fang *et al.* developed a novel organic precursor method to deposit amorphous ruthenium oxide films under 200℃, however, the deposits become crystalline once temperature was raised above 200℃ [8]. Besides, roughness of the deposited films needs to be improved. Furthermore, Rochefort *et al.* used the thermal decomposition to produce RuO_2 film on a Ti substrate with 150 nm thickness for 2 hr at 400℃ in 2003 [25].

Later in 2004, Il-Hwan Kim *et al.* took advantage of electrostatic spray deposition to produce crystalline ruthenium oxide films on different substrates [11]. However, from the cross-sectional image of the deposited films, the deposits does not seem to be sufficiently dense.

2.4 Applications of Ru films

Ruthenium films can be used as the bottom electrode and common plate materials in dynamic random access memories (DRAMs) capacitors because of their low resistivity, excellent chemical stability, and reasonable dry etching property [26]. In addition, the ruthenium has low solubility with copper. Therefore, ruthenium films are of potential to be a diffusion barrier in Cu-metallization [27].

2.5 Fabrications of Ru films

2.5.1 Vacuum deposition

Physical Vapor Deposition (PVD)

Ruthenium is a conductive metal, so most reports related to the ruthenium films deposited by PVD used a sputtering approach [3, 6, 28, 29]. In 2003, Josell *et al.* used the PVD to fabricate Ru films on titanium adhesion layer trenches [3]. However, the deposited films were discontinuous, and the step coverage and films continuity required optimization. On the other hand, a 5 nm amorphous ruthenium film was deposited on a silicon planar substrate by Arunagiri *et al.* with sputtering in 2005 [28].

Later in 2007, Jia *et al.* reported ruthenium films fabricated by dc sputtering [29]. Nevertheless, the deposits were oxidized to form ruthenium dioxide at elevated temperature under oxygen atmosphere. Recently, Onogawa *et al.* [6] have reported amorphous ruthenium/polycrystalline ruthenium on silicon oxide with sputtering.

Chemical Vapor Deposition (CVD)

Compared with ruthenium deposited by the PVD, using the CVD to deposit ruthenium film has several advantages such as ultra thin, highly conformal, and continuous ruthenium films [4]. In ruthenium films from CVD technique, the MOCVD was used with different ruthenium precursors to produce desirable deposits. In addition, the most common substrate used in this method was silicon oxide substrate. In 2004, Cho *et al.* used $Ru(EtCp)_2$ as a precursor to deposit polycrystalline Ru films on silicon oxide [4]. Besides, in 2005, Kang *et al.* used RuCp(*i*-PrCp) precursor with CVD to deposit ruthenium films on five different substrates [5]. Moreover, Kawano *et al.* used Ru(DMPD)(EtCp) as a precursor to produce polycrystalline ruthenium films on SiO_2 substrates in both planar and trenched forms [26]. Recently in 2007, Shin *et al.* used *cis*-$RuH_2(PMe_3)_4$ to produce amorphous Ru-P alloy films on SiO_2 [30].

Although the CVD has some advantages to deposit ruthenium films, undesirable long incubation time and substrates specific dependency are two primary challenges in the CVD to produce ruthenium films [31].

Atomic Layer Deposition (ALD)

In comparison to CVD technique, the ALD has some benefits to deposit

ruthenium films such as better step coverage and thickness control [27]. In 2003, Aaltonen *et al.* grew polycrystalline ruthenium films on borosilicate glass substrates with $RuCp_2$ precursor [32]. Another precursor, 2,4-(dimethylpentadienyl)(ethylcoclopentadienyl)Ru, which is also called DER, was used by Seong Keon Kim *et al.* with the ALD on four different substrates in 2007 [27]. However, the ALD process exhibited poor nucleation at the initial stage of the film growth. Therefore, recently Heo *et al.* took advantage of the UV-O_3 surface treatment to overcome this problem using identical precursor [31].

2.5.2 Solution deposition

Electrodeposition

Some research results have been reported for ruthenium films by the electrodeposition method. In 1997, Chen *et al.* used $RuCl_3$ as a precursor to deposit three monolayer ruthenium by electrodeposition [33]. Recently in 2006, Young-Soon Kim *et al.* took advantage of a N-bridged complex of ruthenium(IV) nitrosyl chloride formed in the plating solution to deposit ruthenium films on Ti and TiNx patterned substrates [34]. From XRD results in their study, diffraction peaks of ruthenium with broad widths suggested the deposited films were poor crystallinity. Later in the same year, this group also reported a 30 nm ruthenium thin film with grain size less than 10 nm was deposited on a titanium substrate with root mean square roughness of 8.3 nm [35]. Unfortunately, roughness for the deposited ruthenium film needed further improvement. In 2008, Thambidurai *et al.* used electrochemical method to deposit ruthenium films with surface limited redox replacement on Au substrates. Pb atomic layers were used in the surface limited redox replacement to control the thickness of

ruthenium nanofilms [36].

Electroless plating (ELD)

The components for the electroless Ru plating bath have been described in several studies. Table 2.2 provides the component of electroless Ru plating bath A, which was the earliest literature report for electroless Ru deposition [15]. It described four different recipes for the ruthenium plating baths. Take solution A–1 for example, the Ruthenium electroless deposition was performed in basic condition under 40℃ on copper sheet. In addition, other examples for the plating solutions were listed in Table 2.2 as well. Table 2.3 presents recent research in 2008 by Lasczek *et al.* for components in their ruthenium electroless plating bath [18], which we defined as the plating bath B. The components for plating bath B were similar to that of plating bath A–1 but differed in substrates. Though functions for individual component were explained carefully, relevant deposition mechanism and qualitative measurements were lacking in their study.

Another recipe for the ruthenium electroless plating was proposed by Okuno in 1990, as listed in Table 2.4 (plating bath C) [16]. The components for electroless Ru plating bath revealed negligible variation from what were listed in Table 2.2 and Table 2.3. The properties of the deposited films were examined after exposure to corrosive gases or solutions. However, qualitative characterization for the as-deposited films was still not performed.

Later in 1991, Chang *et al.* reported ruthenium electroless deposition with a novel plating bath recipe on silicon substrates, as shown in Table 2.5 (plating bath D) [17]. Despite reactions between the components were verified as electroless

deposition by measurement of mixed potentials, specific compounds for the addition agent was absent in Table 2.5. Moreover, we reckon that the deposition mechanism and qualitative measurement can be further investigated. On the other hand, in 2001, Ramani *et al.* used identical recipe except adding the addition agent in Table 2.5 described previously to deposit ruthenium particles on carbon substrates [9]. Therefore, it can be concluded that ruthenium is successfully deposited without addition of the addition agent.

Table 2.2 Components of the electroless Ru plating bath A [15].

		Soln. A–1	Soln. A–2	Soln. A–3	Soln. A–4
Metal precursors	$RuCl_3 \cdot 3H_2O$	2.6 g	2.6 g	–	–
	$K_2[Ru(NO)Cl_5]$	–	–	3.8 g	–
	$[Ru(NO)(NH_3)_5]Cl_3$	–	–	–	3.2 g
Sodium natrite	$NaNO_2$	2.5 g	2.5 g	–	–
Ammonium hydroxide	NH_4OH (28 wt% NH_3)	20 mL	20 mL	20 mL	–
Hydroxylamine hydrochliride	$NH_2OH \cdot HCl$	–	1.0 g	1.0 g	1.5 g
Hydrochloric acid	HCl	–	1.0 g	1.0 g	1.5 g
Hydrazine hydrate	N_2H_4 40 wt%	0.5 mL	–	–	5 mL
pH 12 buffer	0.1 M NaOH plus 0.1 M Na_2CO_4	–	–	–	30 mL
pH		11.8	–	–	12
Temperature		40℃	–	–	40 – 50 ℃
Substrate		Cu	ABS plastic	–	–

Soln. A–1 Dissolve $RuCl_3 \cdot 3H_2O$ in 50 mL H_2O. Add a few drops of HCl and $NaNO_2$ in small increments and boil. Add NH_4OH and heat to boil. Dilute to 500 mL after cooling.

Soln. A–2 As above, except that NH_4OH and hydroxylamine are added at the same time instead of NH_4OH alone.

Soln. A–3 Add hydroxylamine after boiling mixture of Ru-salt and NH_4OH. Then dilute to 500 mL.

Soln. A–4 Add Ru-salt in the buffer and heat for dissolution. Add hydroxylamine and dilute to 500 mL.

Table 2.3 Components of the electroless Ru plating bath B [18].

Ruthenium chloride	$RuCl_3 \cdot xH_2O$	0.208 g/80 mL
Sodium natrite	$NaNO_2$	0.2 g/80 mL
Ammonium hydroxide	NH_4OH, (28 wt% NH_3)	30 mL/80 mL
Sodium hydroxide	NaOH	1 g/80 mL
Hydrochloric acid	HCl	0.04 mL/80 mL
Hydrazine hydrate	N_2H_4	0.75 mL/80 mL
pH		12.8
Temperature		55℃
Substrate		Pd-InGaAs

Table 2.4 Components of the electroless Ru plating bath C [16].

Ruthenium salt		2.0 g/L
Ammonium hydroxide	NH_4OH, (28 wt% NH_3)	37.5–150 mL/L
Sodium hydroxide	NaOH	5–60 g/L
Hydrazine hydrate	N_2H_4	1–6.5 g/L
pH		12.6–13.6
Temperature		55–65℃
Substrate		Cu

Table 2.5 Components of the electroless Ru plating bath D [9, 17].

Reference	[17]	[9]
$RuCl_3 \cdot xH_2O$ (40.88 wt%)	0.014 M	0.014 M
$C_6H_{14}N_2O_7$	0.014 M	0.014 M
$H_4NOCOCOONH_4 \cdot H_2O$	0.07 M	0.07 M
NaOH	Small amount	Small amount
$NaH_2PO_2 \cdot H_2O$	0.27 M	0.27 M
Addition agent	Small amount	–
pH	9.5	9.5
Temperature	85℃	90℃
Substrate	Si	C

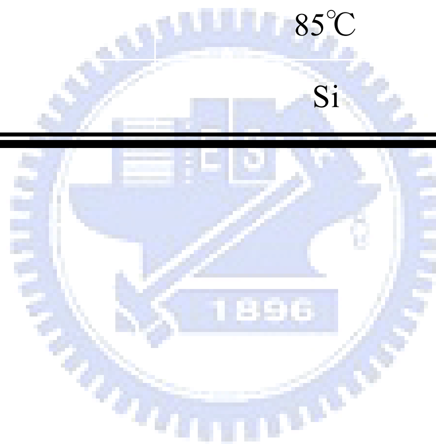

Chapter 3 Experimental

3.1 Experimental design

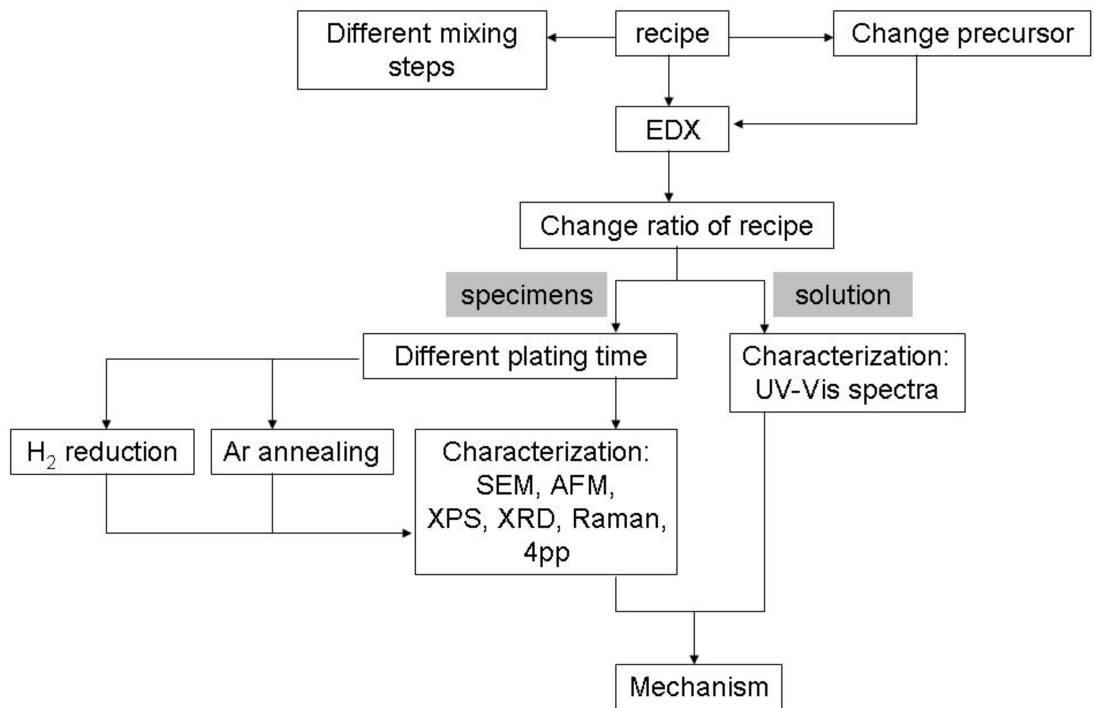

Figure 3.1 Experimental flowchart.

3.2 Materials

Table 3.1 Materials used in this research.

Materials	Purity
$K_2RuCl_5 \cdot xH_2O$ (Alfa Aesar)	Ru: 25.4 wt%
$NaNO_2$ (SHOWA)	97 wt%
NaClO (SHOWA)	active Cl: 5–6 wt%
NaOH (Mallinckrodt)	99 wt%
$PdCl_2$ (Aldrish)	>99 wt%
HCl (SHOWA)	35–37 wt%
H_2	99.999 wt%
Ar	>99 wt%
Cu substrate	

3.3 Plating bath preparation

Cu specimen was used as the substrate during Ru electroless plating process. The structures and thickness of Cu substrate is shown in Figure 3.2. First, the Cu substrate was rinsed with acetone and water to remove impurities. Before immersing into the plating bath, the specimen was dipped into $PdCl_2$ aqueous solution for 10 sec at 40℃ for activation process. The components of $PdCl_2$ aqueous solution included 0.1 wt% $PdCl_2$ and 0.1 wt% HCl. The size of Cu substrate was 2×2 cm^2. The total volume of

plating bath was 30 mL aqueous solution which including $K_2RuCl_5 \cdot xH_2O$, $NaNO_2$, NaOH, and NaClO. The formulation was listed in Table 3.1.

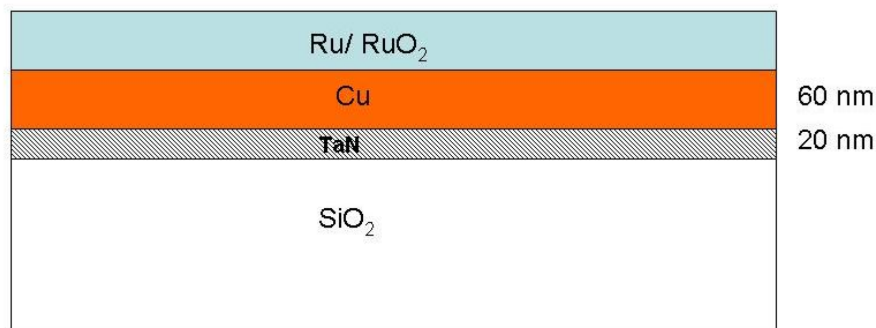

Figure 3.2 Structures of the substrate for electroless plating.

Table 3.2 Bath components and operating condition for the electroless plating.

	Materials	Amount	Corresponding Concentrations
Metal precursor	$K_2RuCl_5 \cdot xH_2O$	0.0186 g / 30 mL	1.73×10^{-3} M
Reducing agent	$NaNO_2$	0.7038 g / 30 mL 0.0704 g / 30 mL 0.0352 g / 30 mL	0.34 M 0.034 M 0.017 M
Stabilizer	NaOH	0.04 g / 30 mL	0.033M
Oxidizing agent	NaClO	2 mL / 30 mL	
	pH		11–12
	Temperature		40℃

The Ru plating solution was prepared by following procedure. Figure 3.3 illustrates the adding process. To begin with, $NaNO_{2\,(aq)}$, $NaOH_{(aq)}$, and $NaClO_{(aq)}$ were mixed together into one solution. Then the mixture was added into the Ru precursor solution at room temperature. After mixing 3 min, the plating bath turned yellow. And it gently turned orange after another 4 min. Once the plating bath turned orange, the plating bath was ready for deposition. At this moment, the pH value of the plating bath was in range from 11 to 12. And then the activated Cu substrate was dipped into the plating bath for ruthenium electroless plating with a variety of plating time at 40℃ under water bath environment. The deposition temperature was 40℃ instead of room temperature because the deposition rate at room temperature was slower than that at 40℃. After finished the plating process, the sample was moved to room temperature for 40 min in air cooling to prevent film failure by thermal stress.

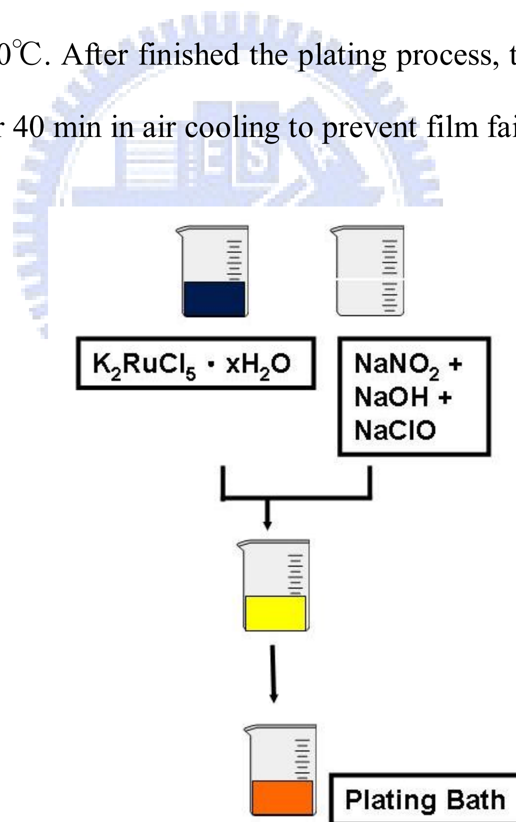

Figure 3.3 The adding steps of the plating bath.

3.4 Instruments and characterization

UV-Vis spectrometer

UV-Visible spectrometer (UV-Vis: Agilent 8453) was used to measure the absorption spectra of the deposition solution.

EDX

Specimens were examined by Energy Dispersive Spectrometer (EDX: JSM6500F) to check if the Ru was successfully deposited.

SEM

The morphology and thickness of the deposited thin films were obtained by a field emission scanning electron microscope (FESEM: JSM6500F or JSM6700). Ag conductive layer was coated by evaporation on the deposited films to prevent charging during measurements.

AFM

The grain size and roughness of the deposited films were measured by an atomic force microscope (AFM: Vecco Dimension 5000 Scanning Probe Microscopy).

XPS

The oxidation states of ruthenium and oxygen on the deposited films were identified by X-ray Photoelectron Spectrometer (XPS: Thermo Microlab 350).

XRD

X-ray diffractometer (HRXRD: BedeD1) was used to determine relavent phase and crystallinity of the deposited films.

Raman

Raman spectrometer was used to characterize the deposited films (Raman spectrometer LabRAM HR800).

4pp

The resistivity of the deposited films was measured by a four-point probe (CMT-SR2000N).

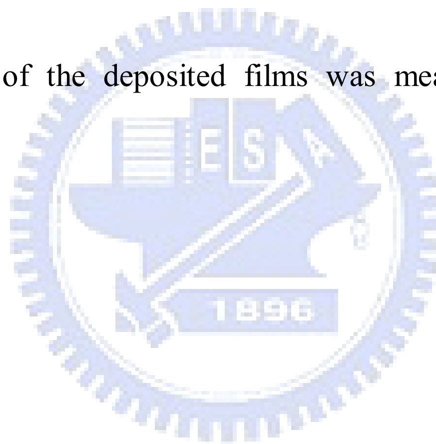

Chapter 4 Results and Discussion I: Development of Ru electroless plating solution

4.1 Development of plating bath components

$K_2RuCl_5 \cdot xH_2O$, and $RuCl_3 \cdot xH_2O$ were the most common chloride-containing compounds among ruthenium precursors. Between them, $RuCl_3 \cdot xH_2O$ was widely used in ruthenium related reactions. However, in most cases using the $RuCl_3 \cdot xH_2O$, a small amount of hydrochloride acid (HCl) was added to promote $RuCl_3 \cdot xH_2O$ dissolution in water. Therefore, in our study, the $K_2RuCl_5 \cdot xH_2O$ was used instead to formulate the plating bath because of its direct dissolution in water.

Figure 4.1 depicts four different mixing steps and corresponding color change for the plating baths. In Figure 4.1, all the solutions turned orange once preparation steps were complete. In comparison to Figure 3.3, these results suggested that during the plating solution preparations, the adding sequence of $NaNO_{2(aq)}$, $NaOH_{(aq)}$, and $NaClO_{(aq)}$ bears negligible effect. However, the adding steps described in Figure 4.1 were much more complicated than that in Figure 3.3. Therefore, the adding steps in Figure 3.3 were selected in this study because of their relative simplicity.

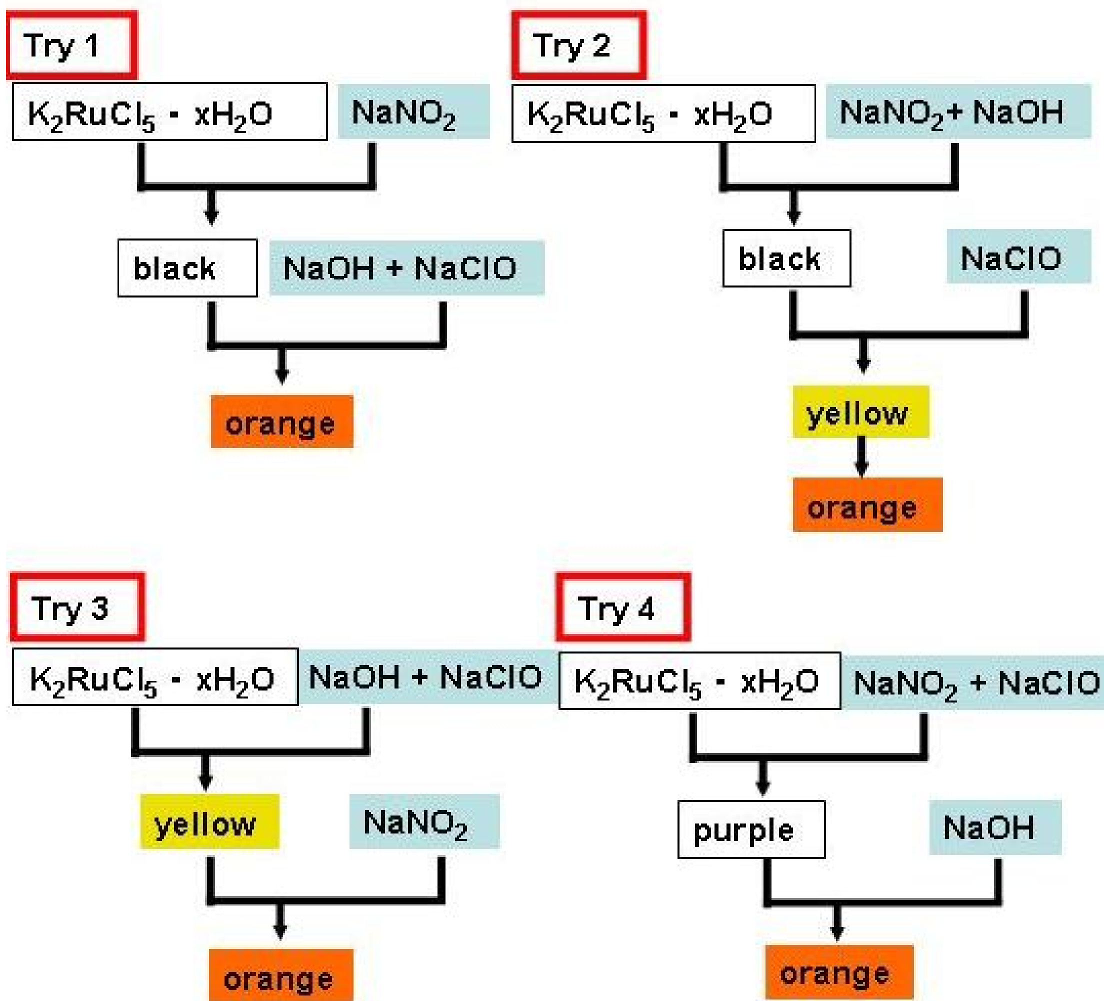

Figure 4.1 Four different adding steps for the plating bath.

It is known that a pale yellow $RuO_{4(aq)}$ can be formed by reaction between ruthenium precursor and sodium hypochlorite (NaClO) [37, 38]. However, because of relatively instability in sodium hypochlorite, a small amount of sodium hydroxide (NaOH) was added in sodium hypochlorite solution to prevent the dissociation of sodium hypochlorite [20]. The molar ratio for sodium hydroxide and sodium hypochlorite was fixed at 0.28 in this research because of results from previous investigation in our group [39]. Previously, the sodium nitrite ($NaNO_2$) was used as a complex agent [15]. However, earlier work also used hydrazine hydrate (N_2H_4) as a reducing agent in electroless plating bath. Nevertheless, in this research, the sodium

nitrite, $NaNO_{2(aq)}$ was found to possess promising ability to serve as a reducing agent in addition to a complexing agent.

To figure out the role of sodium nitrite in the plating bath, three different concentrations of $NaNO_2$ were selected to develop plating solutions in 0.6, 0.06, and 0.03 M, respectively. The corresponding molar ratio for NaClO and $NaNO_2$ was 0.35, 3.5, and 7, respectively.

4.2 Deposition mechanism

The deposition mechanism was proposed by the following equations, which can be further divided into two stages;

The first stage:

$$6OH^-_{(aq)} + 2RuCl_5^{2-}{}_{(aq)} + 5ClO^-_{(aq)} \rightarrow 2RuO_{4(aq)} + 15Cl^-_{(aq)} + 3H_2O_{(l)} \quad (1)$$

The second stage:

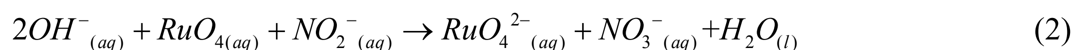

$$2OH^-_{(aq)} + RuO_{4(aq)} + NO_2^-{}_{(aq)} \rightarrow RuO_4^{2-}{}_{(aq)} + NO_3^-{}_{(aq)} + H_2O_{(l)} \quad (2)$$

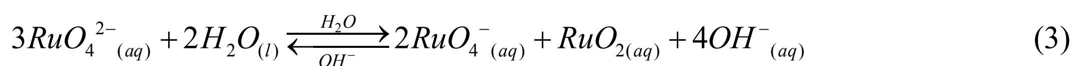

$$3RuO_4^{2-}{}_{(aq)} + 2H_2O_{(l)} \underset{OH^-}{\overset{H_2O}{\rightleftarrows}} 2RuO_4^-{}_{(aq)} + RuO_{2(aq)} + 4OH^-_{(aq)} \quad (3)$$

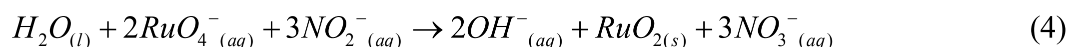

$$H_2O_{(l)} + 2RuO_4^-{}_{(aq)} + 3NO_2^-{}_{(aq)} \rightarrow 2OH^-_{(aq)} + RuO_{2(s)} + 3NO_3^-{}_{(aq)} \quad (4)$$

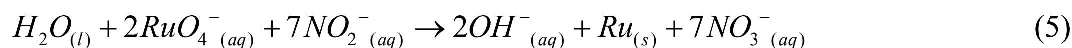

$$H_2O_{(l)} + 2RuO_4^-{}_{(aq)} + 7NO_2^-{}_{(aq)} \rightarrow 2OH^-_{(aq)} + Ru_{(s)} + 7NO_3^-{}_{(aq)} \quad (5)$$

At the first stage, during the initial 3 min right after mixing, the solution turned yellow because of the formation of dissoluble RuO_4, as shown in equation (1).

However, at the second stage during the following 4 min, the solution turned orange slowly. The change of solution color resulted from the reaction between RuO_4 and $NaNO_2$, as shown in equation (2). Although the $NaNO_2$ was commonly used as an oxidizing agent in industry, the RuO_4 has been reported as a strong and poorly-selective oxidant [40]. Compared with the standard reduction potentials of RuO_4 and that of $NaNO_2$, the reaction between RuO_4 and $NaNO_2$ was spontaneous in thermodynamic, in which the RuO_4 was an oxidizing agent and $NaNO_2$ behaved as a reducing agent. In addition, the orange RuO_4^{2-} ion was one of the products in equation (2), and its existence has been confirmed by a UV-Visible spectrum. The spectra of RuO_4^{2-} ions will be further discussed in next section (section 4.3).

In addition, the RuO_4^{2-} ion would underwent a disproporationation reaction to produce RuO_2 deposits and RuO_4^- ions, as shown in equation (3) [38]. Furthermore, following the disproporationation in equation (3), the excess $NaNO_2$ continued to react with the RuO_4^- ions to produce RuO_2 and Ru deposits, as shown in equation (4) and equation (5), respectively.

4.3 Stability of plating solution

To figure out the stability of the plating solution, a UV-Visible spectrometer was used to record the characteristic absorption peaks and the changes of absorption spectra as time progressed. Figure 4.2 displays the UV-Vis absorption spectra under the plating temperature (40 ℃) and room temperature with three different

concentrations of $NaNO_2$. Take Figure 4.2 (b) for example, two absorption peaks in the spectra were clearly observed, one was located between 350 and 375 nm (peak A), and the other was ranged from 460 to 470 nm (peak B). In addition, the absorbance of these two primary absorption peaks in Figure 4.2 (b) was decreased with longer time. Moreover, the absorbance of peak A decayed more rapidly than that of peak B as time progressed.

The curve and the position of absorption peaks from the spectra were consistent with that of RuO_4^{2-} [38]. The position of peak B was consistent with the color of plating bath, which was orange. Furthermore, the absorbance ratios of peak A and peak B were different with different concentrations of sodium nitrite. This result was attributed to the unreacted $NaNO_2$. It was because the sodium nitrite aqueous solution revealed an absorption peak at 350 nm which was near peak A in UV-Visible spectrum [41].

Table 4.1 summarizes the distribution of the two maximum absorption wavelengths in Figure 4.2 for the entire plating bath lifetime. The narrow distribution of the maximum absorption wavelength in the entire plating solution lifespan suggested that the species were stable rather than transforming into other species in the solution. Moreover, the lifetime of stability in Figure 4.2 (b) at 40℃ was relatively shorter compared to that in Figure 4.2 (e) at room temperature.

Figure 4.3 demonstrates the absorbance at 468 nm in UV-Visible spectra with various time under 40℃ and room temperature. With the same concentration of sodium nitrite, the absorbance in Figure 4.3 (a) decreased more rapidly than that in Figure 4.3 (b). This result indicated that the plating rate at 40℃ was faster in comparison to that at room temperature.

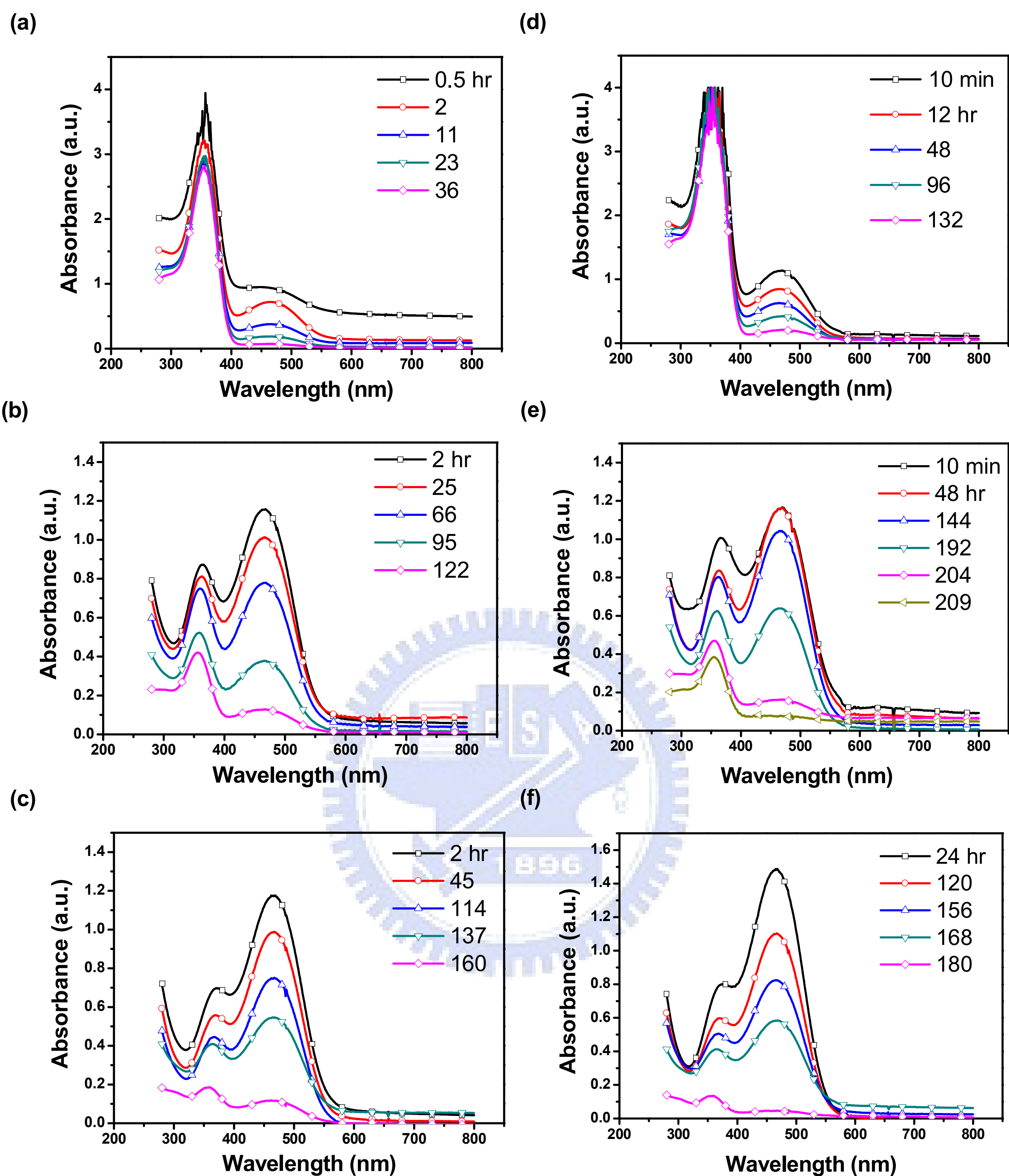

Figure 4.2 UV-Vis spectra of plating baths in three different ratios at various time under 40℃ and room temperature; (a)–(c) are at 40℃, and (d)–(f) are at room temperature; (a) 0.6, (b) 0.06, (c) 0.03, (d) 0.6, (e) 0.06, and (f) 0.03 M $NaNO_{2(aq)}$.

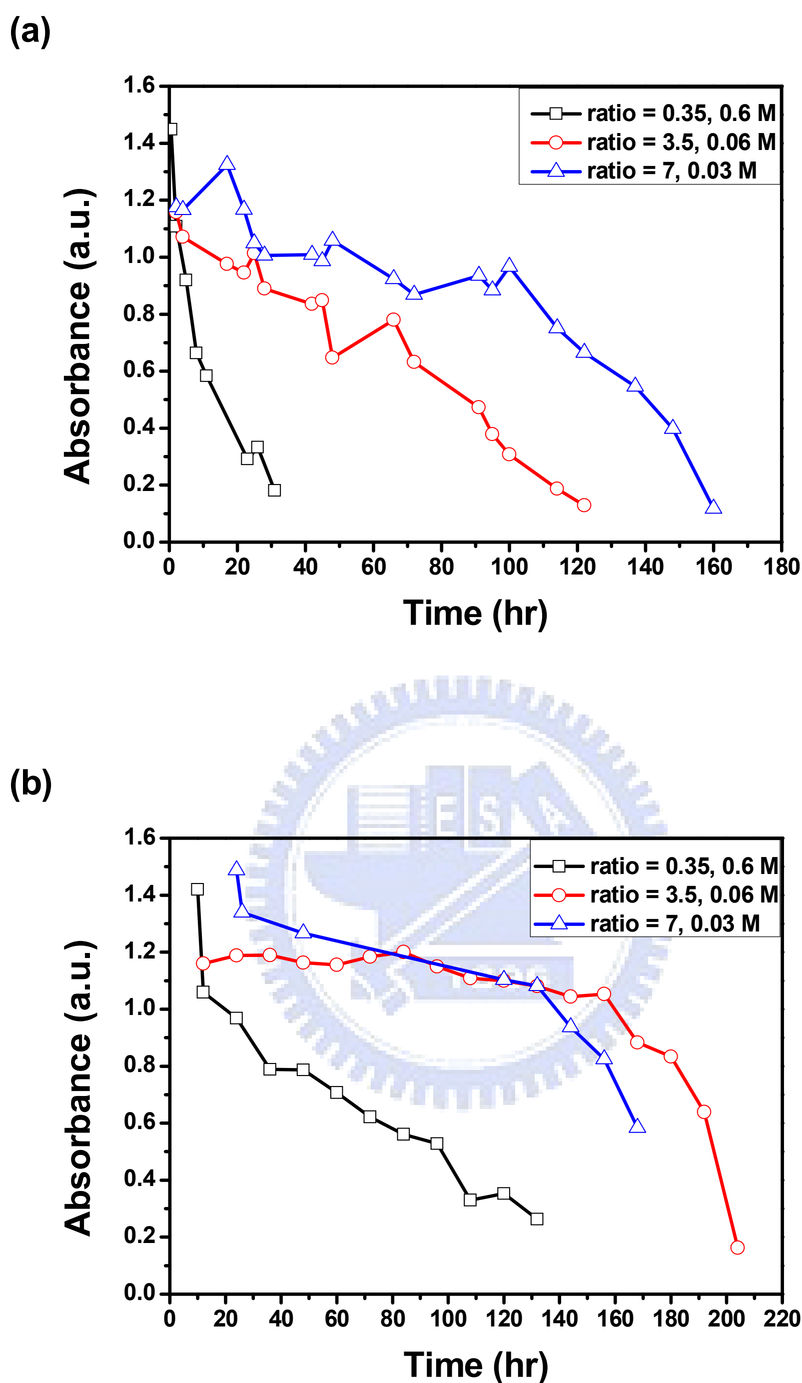

Figure 4.3 Evolution of the absorbance from the maximum absorption wavelength of UV-Vis spectra in various time under different temperatures; (a) at 40 ℃, and (b) at room temperature.

Table 4.1 The distribution of the maximum absorption wavelength between 300 nm and 500 nm.

Concentrations of $NaNO_{2(aq)}$ (at 40℃)	300–400 (nm) (Peak A)	400–500 (nm) (Peak B)
0.03 M	368–373	462–468
0.06 M	357–365	465–468
0.6 M	349–357	463–467

Chapter 5 Results and Discussion II: Characterization of composite RuO_2 and Ru films

5.1 Characterization of composite RuO_2 and Ru films

5.1.1 The existence of Ru element in the deposited films

The results from energy dispersive spectrometer for the deposited films with 0.06 M $NaNO_{2(aq)}$ at various plating time are shown in Figure 5.1. The plating time in Figure 5.1 were 30, 60, and 240 min, respectively. In this research, when the plating time exceeded more than 30 min, the signals from ruthenium were detected by the energy dispersive spectrometer. The atomic percentage of ruthenium in EDX result increased with the plating time. As the plating time was 30 min, the atomic percentage of Ru was 0.77%. When the plating time reached 60 and 240 min, respectively, the atomic percentages of ruthenium increased up to 1.66% and 3.95%. The results suggested a sustained growth of Ru.

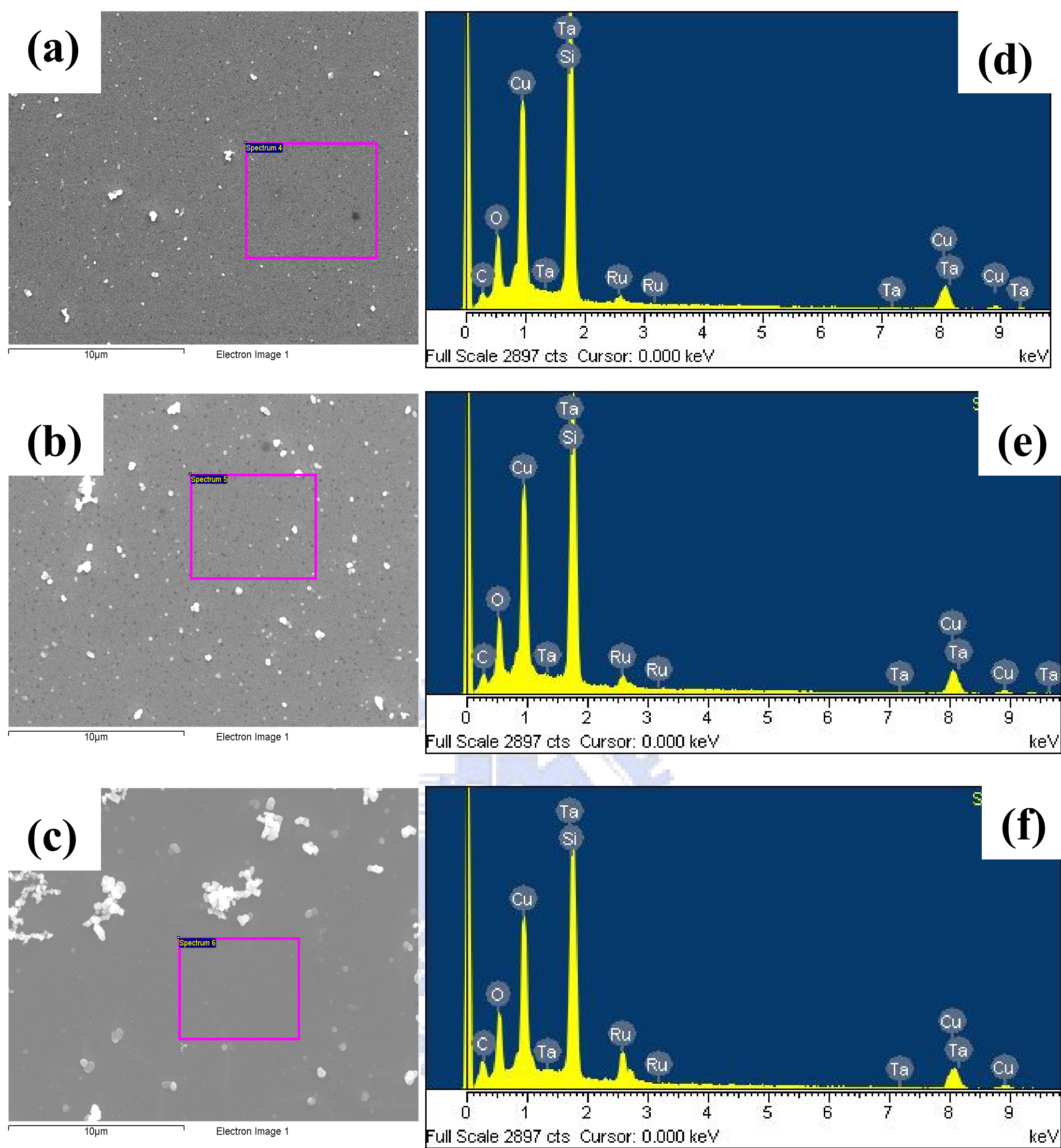

Figure 5.1 EDX results from the deposited films with 0.06 M $NaNO_{2(aq)}$ at various plating time; (a) 30, (b) 60, and (c) 240 min, respectively. (d)–(f) were the corresponding spectrum.

5.1.2 Morphology observation and thickness measurement of the deposited films

Figure 5.2 presents the planar views of deposited films at various plating time with 0.6 M $NaNO_{2(aq)}$. The plating time were 30, 60, 120, 240, and 480 min, respectively. For instance, in Figure 5.2 (a), when the plating time was 30 min, the planar view was uniform with small particles. The existence for these small particles inferred that the deposited films grew continually. This finding was consistent with the results from EDX as described previously. The deposited films remained uniform as the plating time was increased up to 120 min. However, when the plating time was further up to 240 min, films with cracks were easily observed in the SEM image, as shown in Figure 5.2 (d). It was worth noting that the position of cracks was near the location of particles. In addition, the deposited film cracked as the plating time reached 480 min, as shown in Figure 5.2 (e). This finding indicates the cracking on the deposited film is attributed to the internal stress rather than thermal stress because temperature gradient in all samples remains unchanged, which is from 40℃ to room temperature. The results described above were similar to the deposited films with lower concentrations of sodium nitrite, 0.06 and 0.03 M, as shown in Figure 5.3 and Figure 5.4, respectively.

Figure 5.5 provides the cross-sectional views of the deposited films at various plating time with 0.06 M $NaNO_{2(aq)}$. In order to observe the deposited films with cross-sectional views, a silver conducting layer was deposited by evaporation on the deposited films in Figure 5.5 (a) to (d) to prevent the edge charging of SEM. Figure

5.5 (e) was not deposited with a conducting layer because of the crack of deposited film. In addition, Figure 5.5 (f) was the smaller scope of Figure 5.5 (e) for the same sample, in which the deposited film was bended because of a larger internal stress. In Figure 5.5 (a), for example, the cross-sectional view for the deposited film was smooth and the thickness of that was uniform. Besides, the thickness of the deposited films increased with the plating time. It is important to note that the deposited films remain relatively smooth even though the thickness of the deposited films increased with the plating time.

E S A
1896

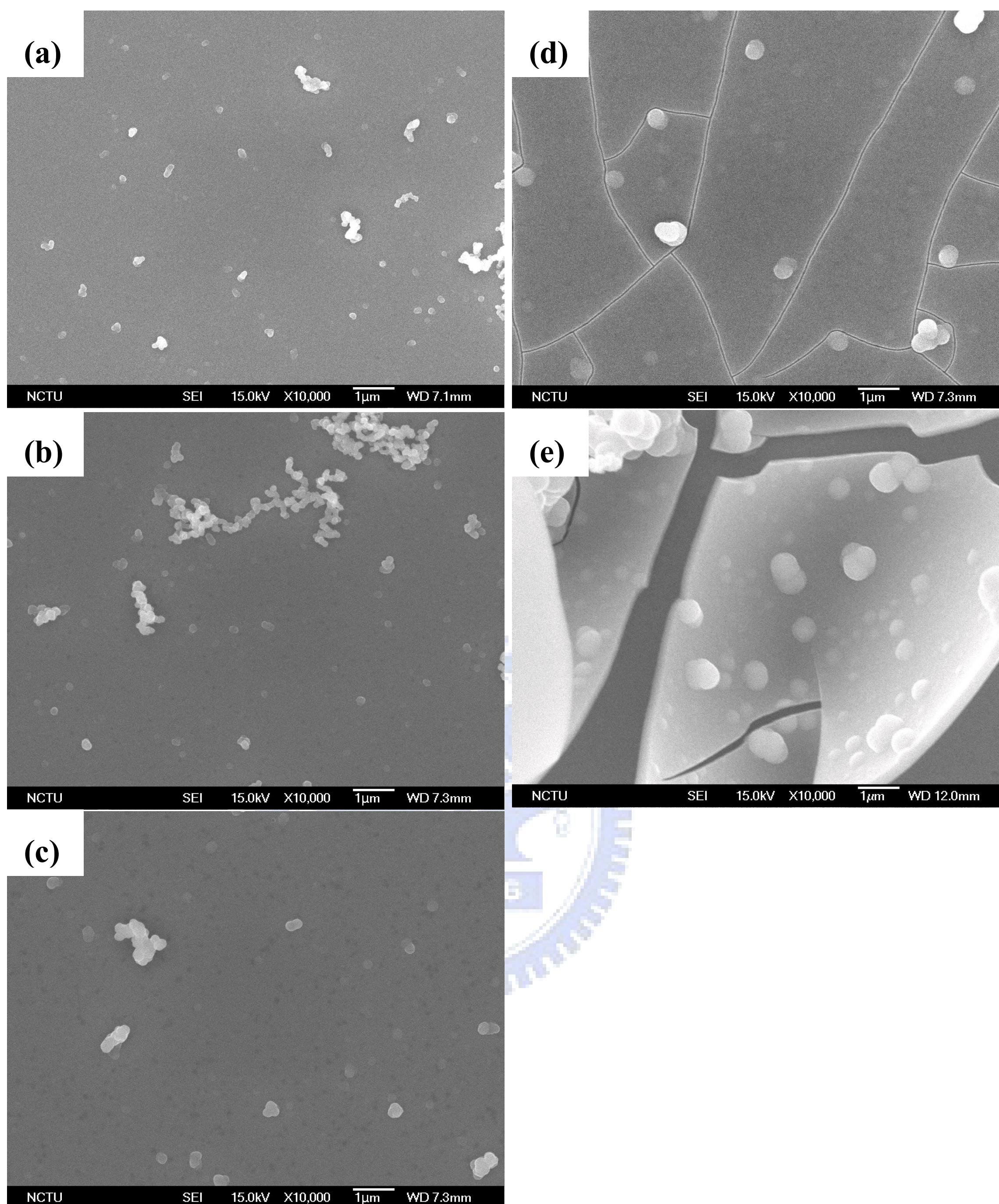

Figure 5.2 Planar views for the deposited films at various plating time with 0.6 M $NaNO_{2(aq)}$; (a) 30, (b) 60, (c) 120, (d) 240, and (e) 480 min, respectively.

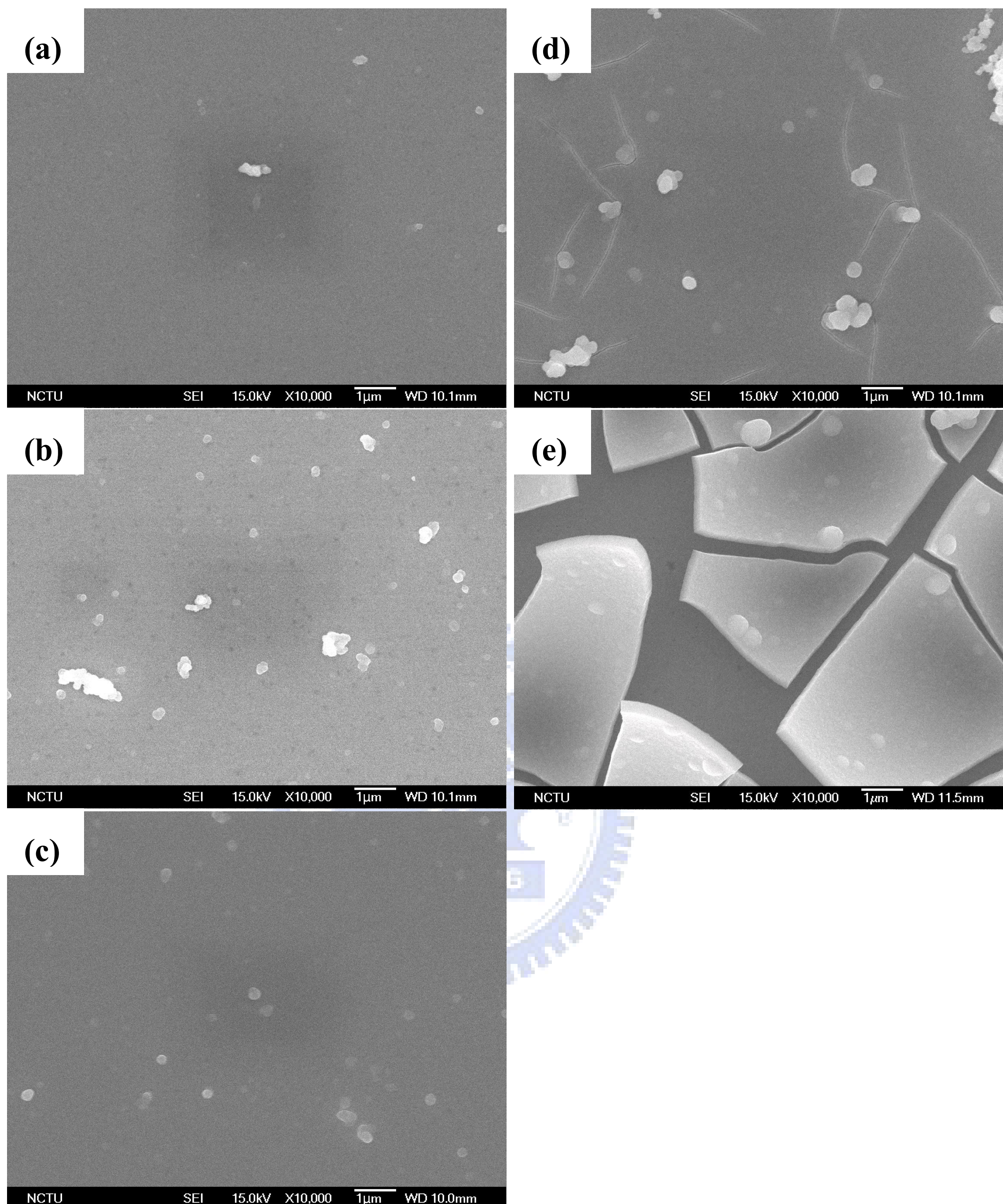

Figure 5.3 Planar views for the deposited films at various plating time with 0.06 M $NaNO_{2(aq)}$; (a) 30, (b) 60, (c) 120, (d) 240, and (e) 480 min, respectively.

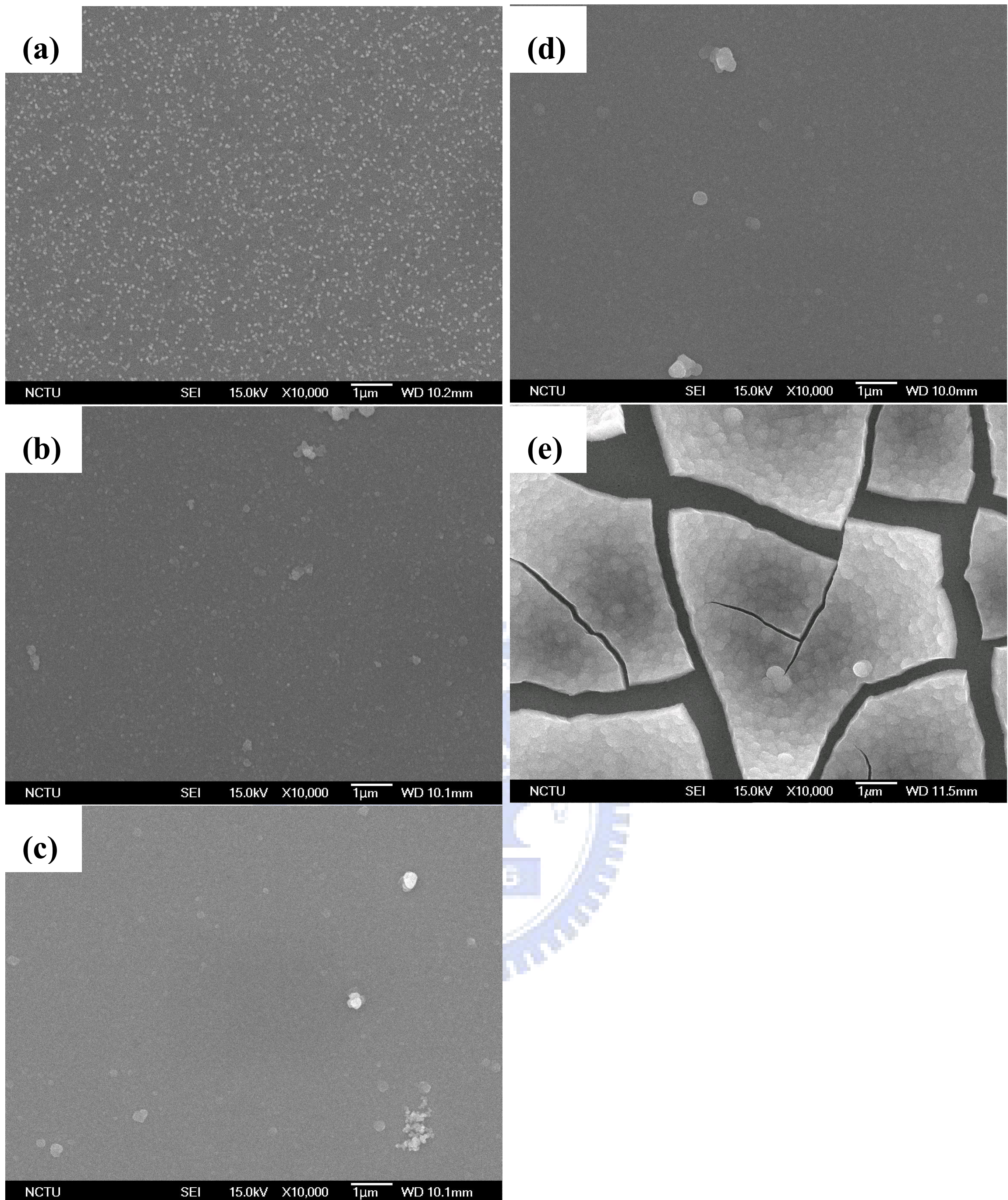

Figure 5.4 Planar views for the deposited films at various plating time with 0.03 M $NaNO_{2(aq)}$; (a) 30, (b) 60, (c) 120, (d) 240, and (e) 480 min, respectively.

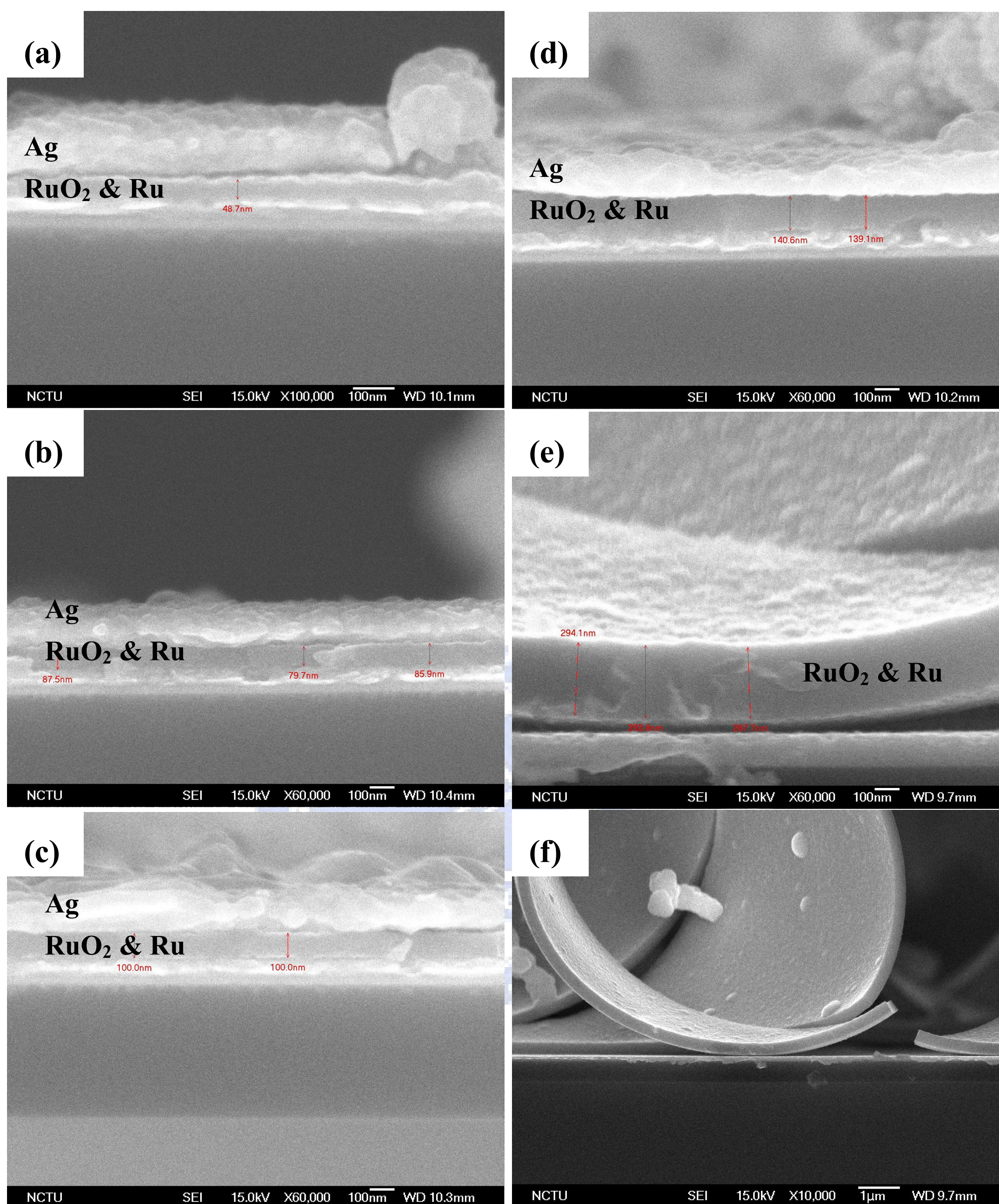

Figure 5.5 Cross-sectional views for the deposited films at various plating time with 0.06 M $NaNO_{2(aq)}$; (a) 30, (b) 60, (c) 120, (d) 240, and (e) 480 min, respectively; and (f) the smaller scope of (e).

5.1.3 Thickness at different plating time

The thicknesses of the deposited films versus various plating time with different concentrations of sodium nitrite are shown in Figure 5.6. The thickness of the deposited film ranged from 35–300 nm at the selected plating time. In addition, the slope in Figure 5.6 revealed the deposition rate at various periods of time with different concentrations of sodium nitrite. As the plating time was increased, the deposition rate gradually decreased. This result was attributed to the reduction of diffusion rate of ruthenium-containing ions in the plating solutions. In other words, the concentration of ruthenium-containing ions decreases with the increasing time, which leads to the reduction of diffusion rate. As a result, the deposition rate is decreased as well.

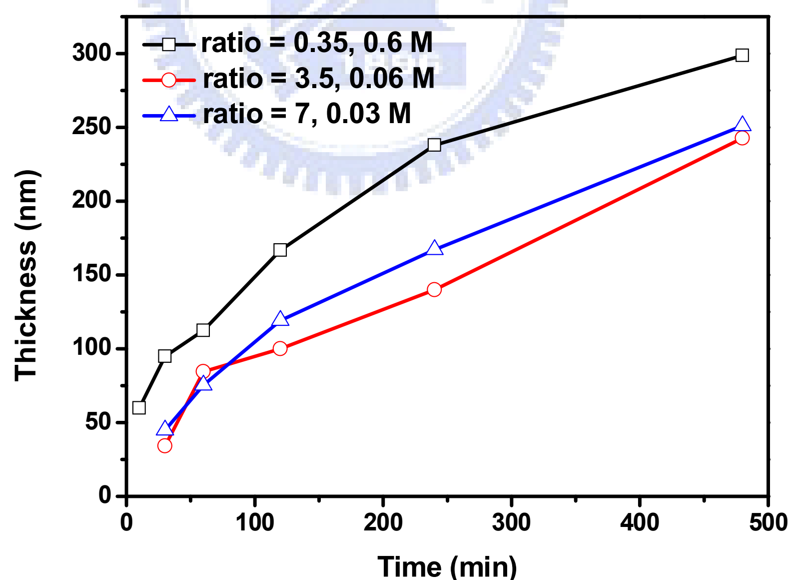

Figure 5.6 Thicknesses for the deposited films versus various plating time with different concentrations of $NaNO_{2(aq)}$.

5.1.4 Roughness measurement for the deposited films

The roughness for the deposited films at three different concentrations of $NaNO_{2(aq)}$ with various plating time are showed in Figure 5.7. The values of root mean square of the roughness (R_q) in the deposited films under selective plating time with various concentrations of $NaNO_{2(aq)}$ were listed in Table 5.1. From Table 5.1, as plating time was increased, the R_q values of the deposited films were increased as well. In addition, when the deposition time was 120 min, the uniformity of the deposited films was decreased with increase of the concentrations of $NaNO_{2(aq)}$, as shown in Table 5.1. Moreover, the uniformity at 120 min plating time with various concentrations of $NaNO_{2(aq)}$ were 2.05%, 4.59%, and 6.70%, respectively. Therefore, combining the results of plating solution lifetime and that of roughness, it is concluded that the recipe for the plating solution with 0.06 M $NaNO_{2(aq)}$ is more applicable than other two concentrations.

Table 5.1 R_q of the deposited films under selective plating time in different concentrations of $NaNO_{2(aq)}$.

Plating time / **Concentration of $NaNO_{2(aq)}$**	**10 min**	**120 min**	**Uniformity at 120 min**
0.6 M	2.358 nm	3.427 nm	2.05%
0.06 M	3.121 nm	4.593 nm	4.59%
0.03 M	2.681 nm	7.977 nm	6.70%

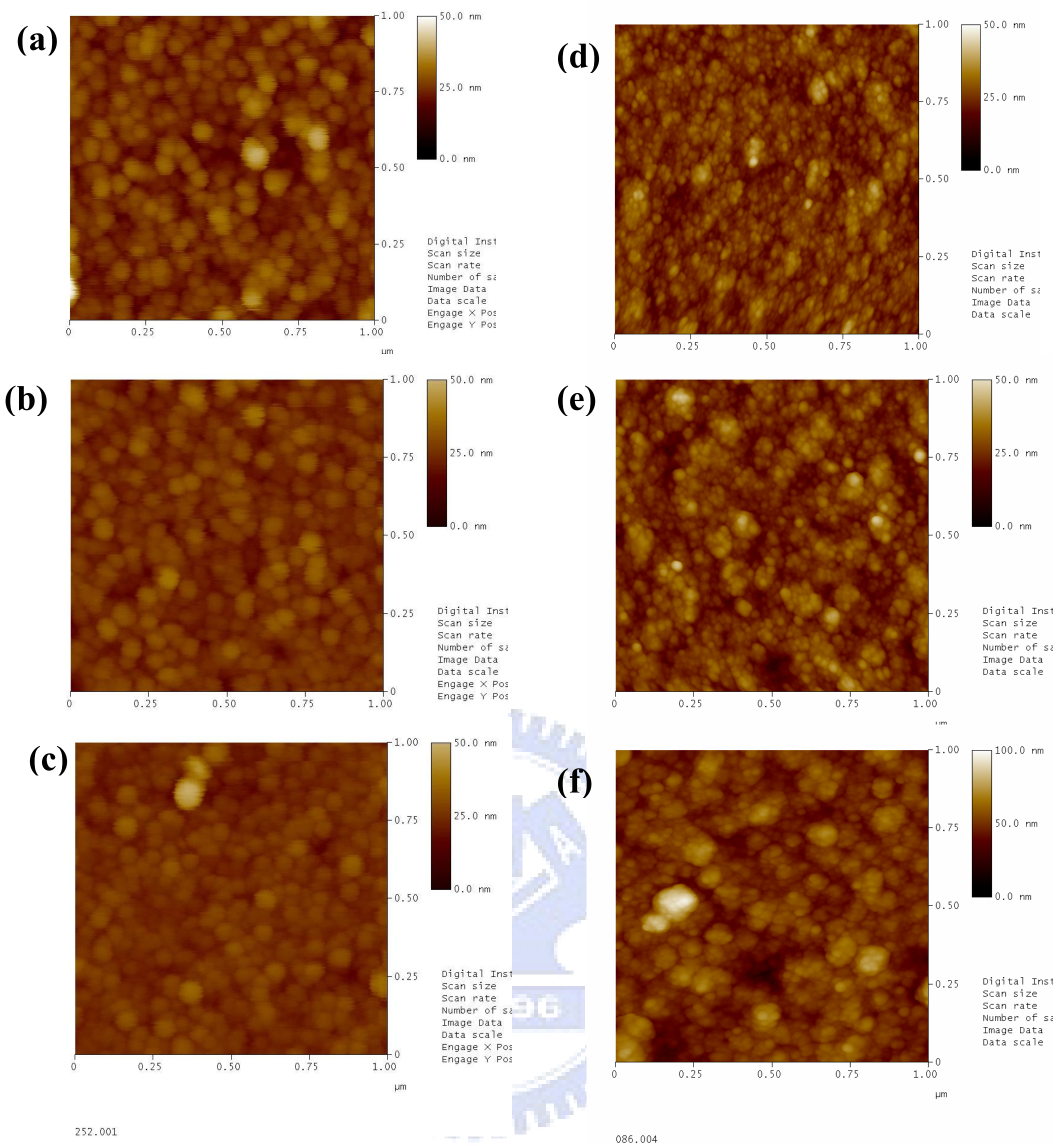

Figure 5.7 Roughness of the deposited films at three different concentrations of $NaNO_{2(aq)}$ in various plating time; (a)–(c) are at 10 min, and (d)–(f) are at 120 min; (a) 0.6, (b) 0.06, (c) 0.03, (d) 0.6, (e) 0.06, and (f) 0.03 M $NaNO_{2(aq)}$.

5.1.5 Characterization of the oxidation states for the deposited films

The oxidation states for the deposited films were determined by the electron spectroscopy for chemical analysis (ESCA), which was measured by a X-ray photoelectron spectrometer. We selected the ruthenium and oxygen to measure, using their spectral lines of 3p3/2 and 1s, respectively. Figure 5.8 provides the XPS spectra of Ru 3p3/2 line for the deposited films with 0.06 M $NaNO_{2(aq)}$ with various plating time, 30, 120, and 480 min, respectively. Similarly, Figure 5.9 displays the corresponding XPS spectra for the O 1s line.

Figure 5.8 exhibits the XPS spectra for the Ru 3p3/2 line from the deposited films at various plating time with 0.06 M $NaNO_{2(aq)}$. From XPS spectra in Figure5.8, a signal of Ru 3p3/2 line was observed, which suggested the presence of ruthenium element in the deposits. This observation was consistent with the results from EDX in Figure 5.1.

In Figure 5.8, the positions of binding energy with maximum intensity in Ru 3p3/2 line were nearly the same. They were located at 464, 464, and 464.2 eV, respectively. This result indicates that the oxidation states for ruthenium from the deposits during the entire plating procedure are identical regardless of the length for the deposition process. The corresponding binding energies with maximum intensity in Figure 5.9 for the O 1s line were at 531.3, 531.1, and 531.2 eV, respectively. This finding suggested that the composition for oxygen in the deposits remained unchanged at different deposition time with the same sodium nitrite concentration.

However, these findings are limited to surface of the deposited films because of shallow depth resolution of XPS. The change of the deposits below depth resolution of XPS during the plating process requires further investigation, such as depth profiling by Auger electron spectrometer (AES).

Furthermore, the entire spectrum for the O 1s line, shown in Figure 5.9 as a shoulder at higher binding energy ranging from 540 to 535 eV, was observed. This result confirms the presence of metal oxides in the deposited films because a shoulder in the O line spectrum is a character for metal oxide. Therefore, this finding indicates that the ruthenium oxides are likely to exist in the deposited films.

To determine the exact compositions for the deposited films, a curving fitting was performed to decide relatively percentage of Ru materials. Figure 5.10 shows the XPS spectra of Ru 3p3/2 line for both experimental and curve fitting lines from the deposited film with 0.6 M $NaNO_2$ for 30 min plating time. From the results of curving fitting, we determined Ru metal, $RuO_2 \cdot nH_2O$, and RuO_3 simultaneous existed in the deposited film. The positions for the binding energy for these three materials were assigned to 462.2, 463.8, and 466.9 eV, respectively. Relative percentages of ruthenium containing materials after the curve fitting in Figure 5.10 were described as follows. The amounts of Ru, $RuO_2 \cdot nH_2O$, and RuO_3 in the deposited film after curve fitting were 11.72%, 68.97%, and 19.31%, respectively, as listed in Table 5.2. The existence of Ru and $RuO_2 \cdot nH_2O$ confirms that the deposited film is a Ru and $RuO_2 \cdot nH_2O$ composite film. However, the existence of RuO_3 in the composite film was a pressing problem. The existence of RuO_3 was attributed to two possible reasons. One possibility for the presence of RuO_3 was that the RuO_3 was formed by surface defects of $RuO_2 \cdot nH_2O$ [10]. The other possibility was that the RuO_3 existed in the

deposited film, acting as an impurity trapped by $RuO_2 \cdot nH_2O$ in the composite film [10].

In comparison to Figure 5.10, Figure 5.11 and Figure 5.12 were the XPS spectra for the Ru 3p3/2 line of experimental and curve fitting from the deposited films for the same plating time with different concentrations of $NaNO_{2(aq)}$, 0.06 and 0.03 M, respectively. The results of curve fitting for the percentage of ruthenium compounds were listed in Table 5.2.

Table 5.2 provides the relative amounts of Ru in different forms in XPS spectra from Figure 5.10 to Figure 5.12. In Table 5.2, as the concentration of $NaNO_{2(aq)}$ was increased, the percentage of RuO_3 was decreased. The result was attributed to the rate of deposition. The deposition rate was increased with increasing concentration of $NaNO_{2(aq)}$. As the concentration of $NaNO_{2(aq)}$ was increased, the concentration gradient was increased in the diffusion layer within the plating solution. Therefore, the ions refilling rate is enhanced with the concentration of $NaNO_{2(aq)}$. In other words, a higher concentration of $NaNO_{2(aq)}$ leads to much less amount of RuO_3 because the rate of ions refilling is expected to be faster.

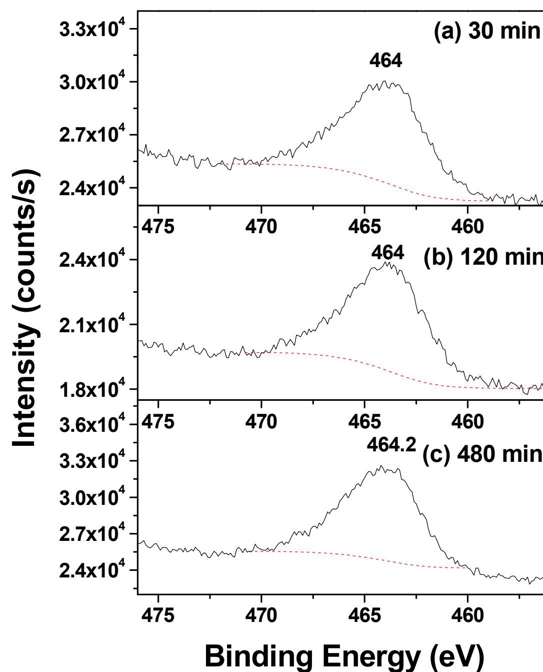

Figure 5.8 XPS spectra for the Ru 3p3/2 line from the deposited films with 0.06 M $NaNO_{2(aq)}$ at various plating time; (a) 30, (b) 120, and (c) 480 min, respectively.

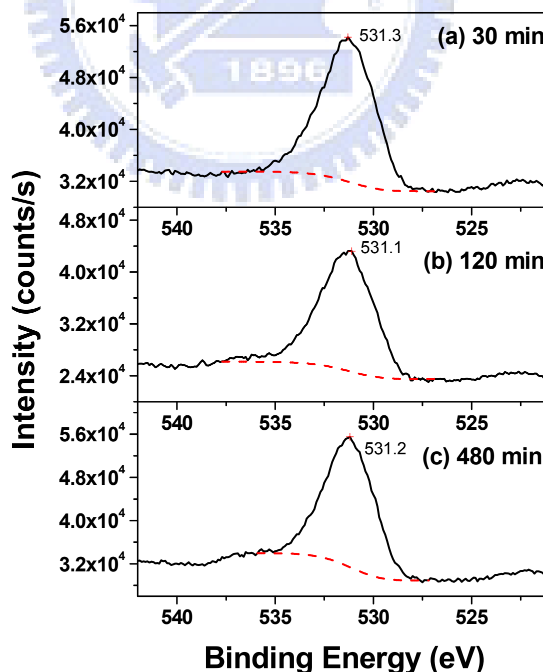

Figure 5.9 XPS spectra for the O 1s line from the deposited films with 0.06 M $NaNO_{2(aq)}$ at various plating times, (a) 30, (b) 120, and (c) 480 min, respectively.

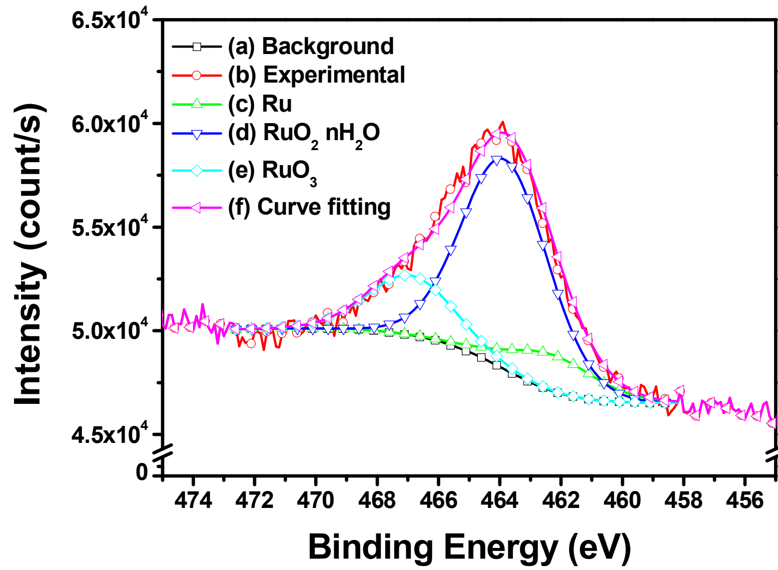

Figure 5.10 XPS spectra for the Ru 3p3/2 line including both experimental and curve fitting of the deposited film with 0.6 M $NaNO_{2(aq)}$ for 30 min plating time.

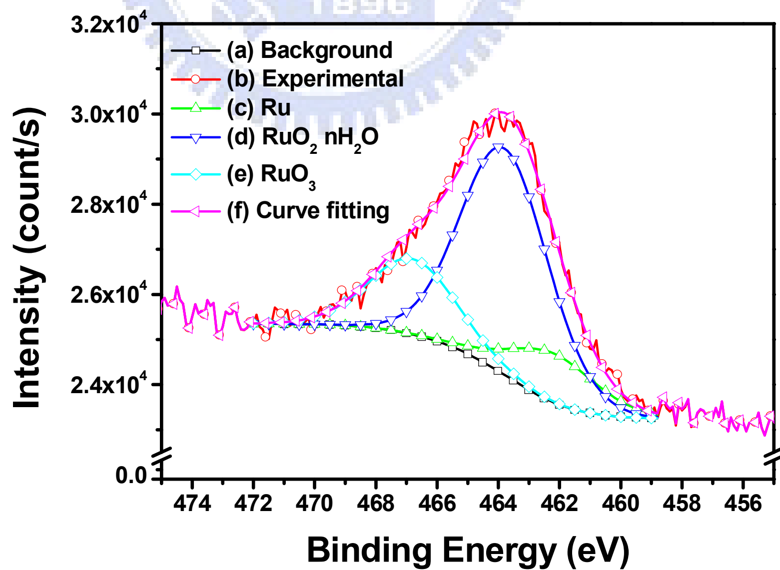

Figure 5.11 XPS spectra for the Ru 3p3/2 line including both experimental and curve fitting of the deposited film with 0.06 M $NaNO_{2(aq)}$ for 30 min plating time.

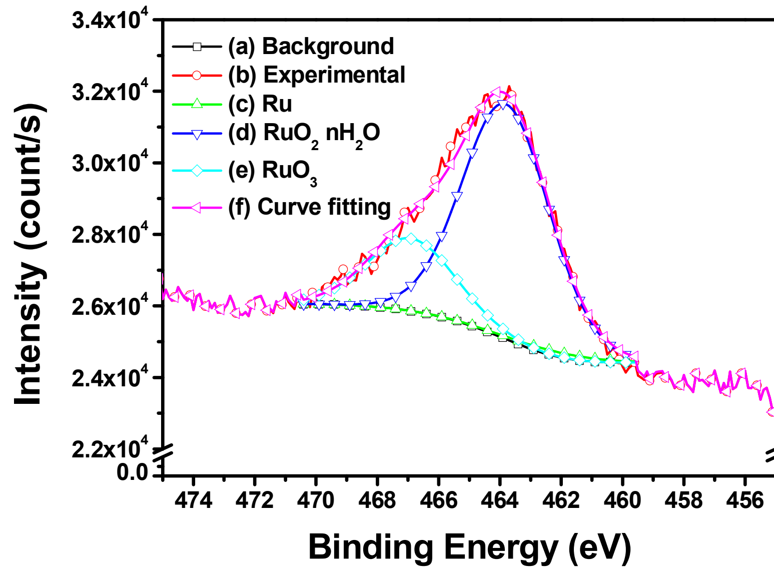

Figure 5.12 XPS spectra for the Ru 3p3/2 line including both experimental and curve fitting of the deposited film with 0.03 M $NaNO_{2(aq)}$ for 30 min plating time.

Table 5.2 Relative amounts of Ru in different forms from XPS spectra from Figure 5.10 to Figure 5.12.

Materials	**RuO_3**	**$RuO_2 \cdot nH_2O$**	**Ru**
	(466.9 eV)	(463.8 eV)	(462.2 eV)
0.6 M	19.31%	68.97%	11.72%
0.06 M	21.29%	64.52%	14.19%
0.03 M	23.31%	75.19%	1.50%

5.1.6 Phase and crystallinity characterization for the deposited films

Figure 5.13 displays the XRD pattern for the as-deposited films with various concentrations $NaNO_{2(aq)}$ for 480 min plating time versus Ru (JCPDS No: 060663) and RuO_2 (JCPDS No: 401290). Because the compositions during the deposition process were identical, the composite films with 480 min plating time for different $NaNO_{2(aq)}$ concentrations were selected to undergo XRD analysis. From Figure 5.13 (a) to Figure 5.13 (c), we did not observe typical crystalline diffraction peaks. Instead, a broad diffraction peak from 30° to 40° was appearing. In addition, in comparison to the standard XRD patterns, we did not observe ruthenium or ruthenium oxide peaks. These results indicated that the as-deposited composite films with different amounts of $NaNO_{2(aq)}$ were amorphous in nature.

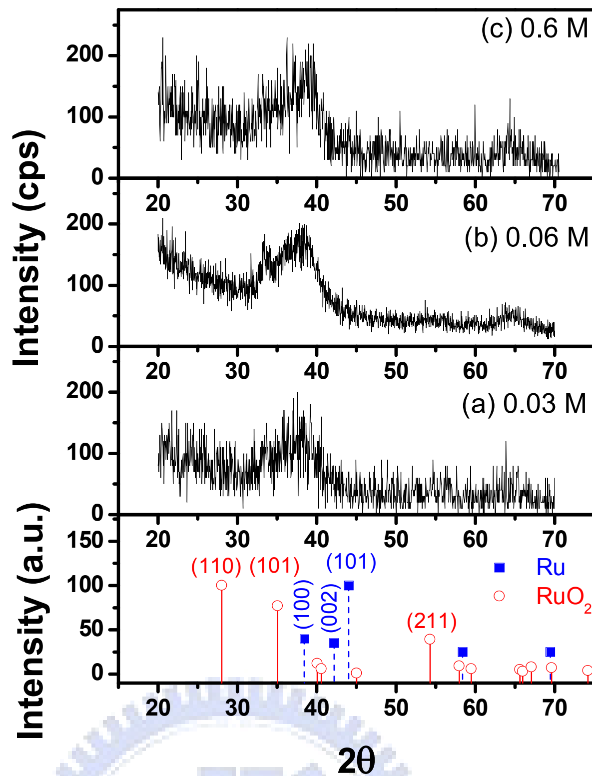

Figure 5.13 XRD patterns for the as-deposited films with various concentrations of $NaNO_{2(aq)}$ for 480 min plating time versus the standard pattern; (a) 0.03 (b) 0.06, and (c) 0.6 M, respectively.

5.1.7 Raman spectroscopy characterization for the deposited films

Raman spectra for the composite films with 0.6 M $NaNO_{2(aq)}$ at various plating time is shown in Figure 5.14. Also displayed is the signal from the Cu stbstrate. As the previous research had suggested, stretching modes of RuO_2 in Raman spectra were located at 515 and 626 cm^{-1}, respectively [33, 42]. From Figure 5.14 (a) and Figure 5.14 (b), a broad peak around 500 cm^{-1} was observed for the composite film with 30

min plating time. Because there was no signal near 500 cm^{-1} for the copper substrate, the 500 cm^{-1} broad peak was attributed to the deposited film. The reasons for its appearance in Figure 5.14 (b) were likely be the existence of ruthenium in the composite films and lattice mismatch at the interface. The existence of ruthenium in the composite films affected the lattice vibration of ruthenium oxide. On the other hand, the lattice mismatch at the interface between the deposited films and the copper substrate produced strain. These reasons led to a broad peak around 500 cm^{-1}, as shown in Figure 5.14 (b). In addition, as the plating time was increased until 240 min, as shown in Figure 5.14 (e), the broad peak was still apparent.

However, as the plating time was increased to 480 min, as shown in Figure 5.14 (f), the Raman spectrum revealed two stretching modes at 506 and 621 cm^{-1}, respectively. Though these peak positions were assigned to ruthenium oxide, which were consistent with those in previous studies [33, 42], the spectrum in Figure 5.14 (f) was notable different from that in Figure 5.14 (b) to (e). This result was owed to the cracking of the composite films. As the plating time was increased to 480 min, the deposited films fell apart as mentioned in Figure 5.2 (e). Because of the crack and following bending of the composite films in Figure 5.14 (f), strain resulted from the lattice mismatch had less contributions at the interface. Therefore, the stretching modes of RuO_2 were observed instead of the broad peak at 500 cm^{-1}.

Furthermore, Figure 5.15 and Figure 5.16 display Raman spectra for the composite films at various plating time with different concentrations of $NaNO_{2(aq)}$, 0.06 and 0.03 M, respectively. As was mentioned above, the results in Figure 5.15 and Figure 5.16 demonstrate a remarkable resemblance to that in Figure 5.14.

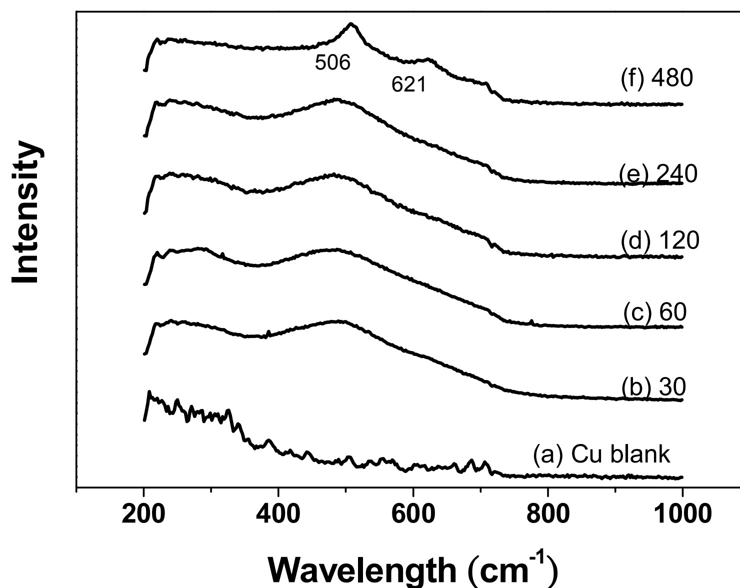

Figure 5.14 Raman spectra for the composite films with 0.6 M $NaNO_{2(aq)}$ at various plating time; (a) Cu substrate as a blank, (b) 30, (c) 60, (d) 120, (e) 240, and (f) 480 min, respectively.

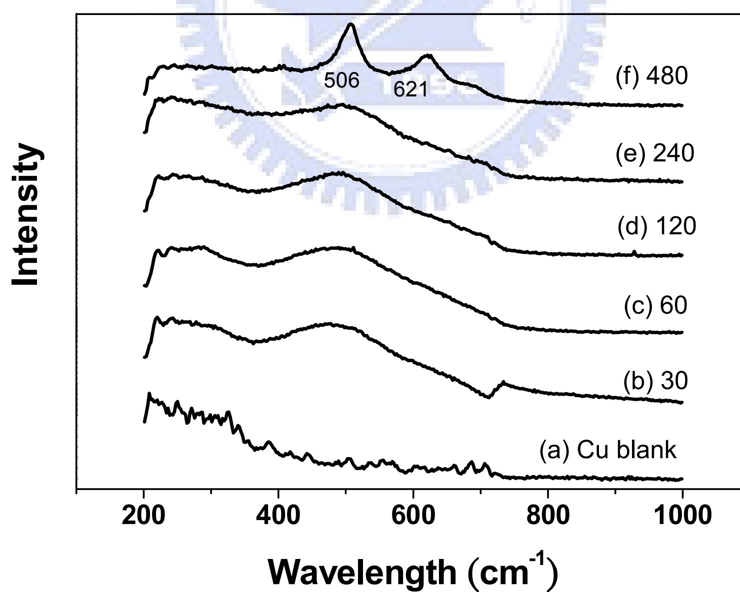

Figure 5.15 Raman spectra for the composite films with 0.06 M $NaNO_{2(aq)}$ at various plating time; (a) Cu substrate as a blank, (b) 30, (c) 60, (d) 120, (e) 240, and (f) 480 min, respectively.

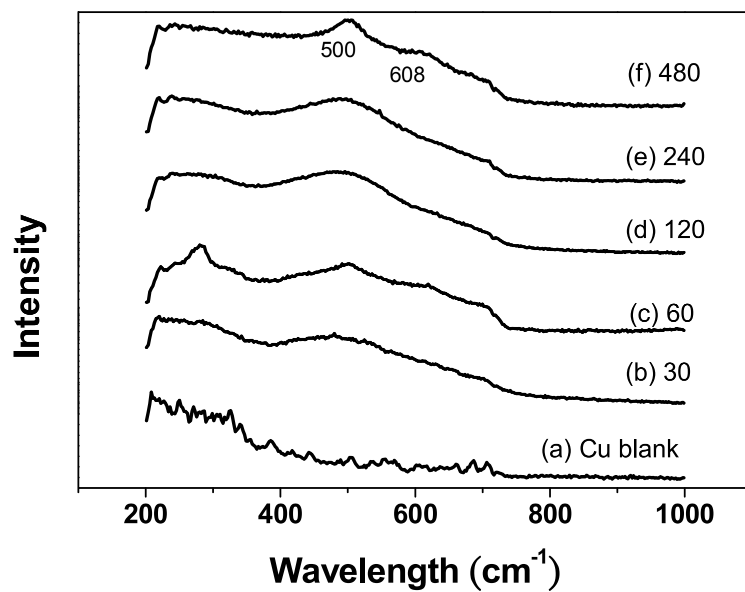

Figure 5.16 Raman spectra of the composite films with 0.03 M $NaNO_{2(aq)}$ at various plating time; (a) Cu substrate as a blank, (b) 30, (c) 60, (d) 120, (e) 240, and (f) 480 min, respectively.

5.2 Characterization of the composite RuO_2 and Ru films after hydrogen reduction

5.2.1 Morphology observation of the deposited films after hydrogen reduction

Figure 5.17 provides the planar views SEM images for the deposited films at various plating time with 0.6 M $NaNO_{2(aq)}$ after hydrogen reduction at 200℃ for 2 hr. In comparison to the composite films in Figure 5.2 at identical plating time, planar views of the composite films after H_2 reduction revealed surface holes. The formation of surface holes was likely from the reduction of ruthenium oxide in the composite films. As the as-deposited films underwent a reduction reaction by H_2, the ruthenium oxide in the deposited films became metallic ruthenium. This reaction led to volume shrinkage of the deposited films. In addition, the formation of surface holes probably suggested roughness in the films would become larger than that of the as-deposited films. On the other hand, as the plating time increased, the number of surface holes in the deposit per unit area was increased as well. This result is attributed to more ruthenium oxide reduction. Because thickness for the composite films increased with the plating time, more ruthenium oxide was reduced at the same unit area. Therefore, the number of the surface holes in reduced films increased with the plating time. Similarly, the same results were observed in Figure 5.18 and Figure 5.19.

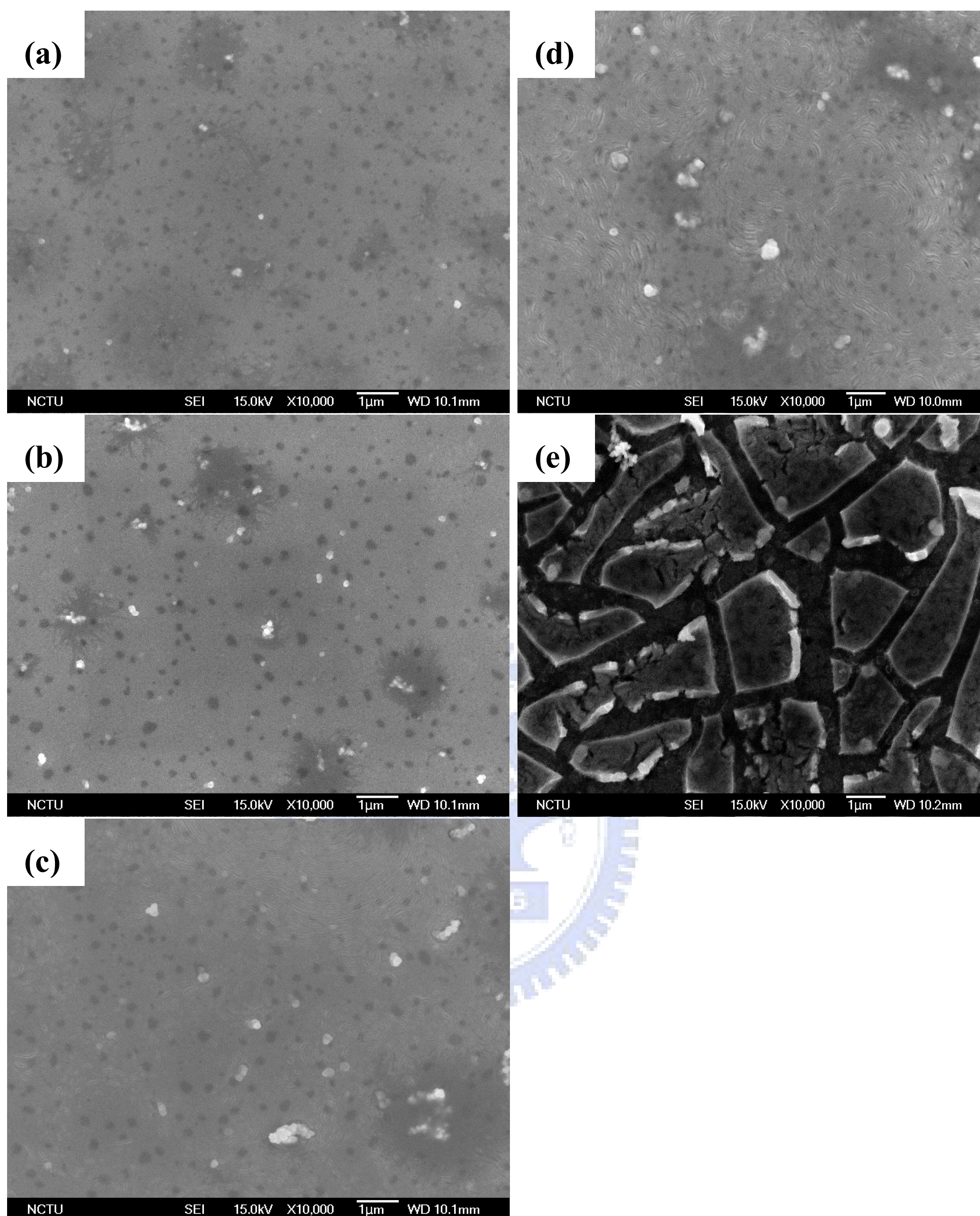

Figure 5.17 Planar views for the deposited films at various plating time with 0.6 M $NaNO_{2(aq)}$ after H_2 reduction at 200℃ for 2 hr; (a) 30, (b) 60, (c) 120, (d) 240, and (e) 480 min, respectively.

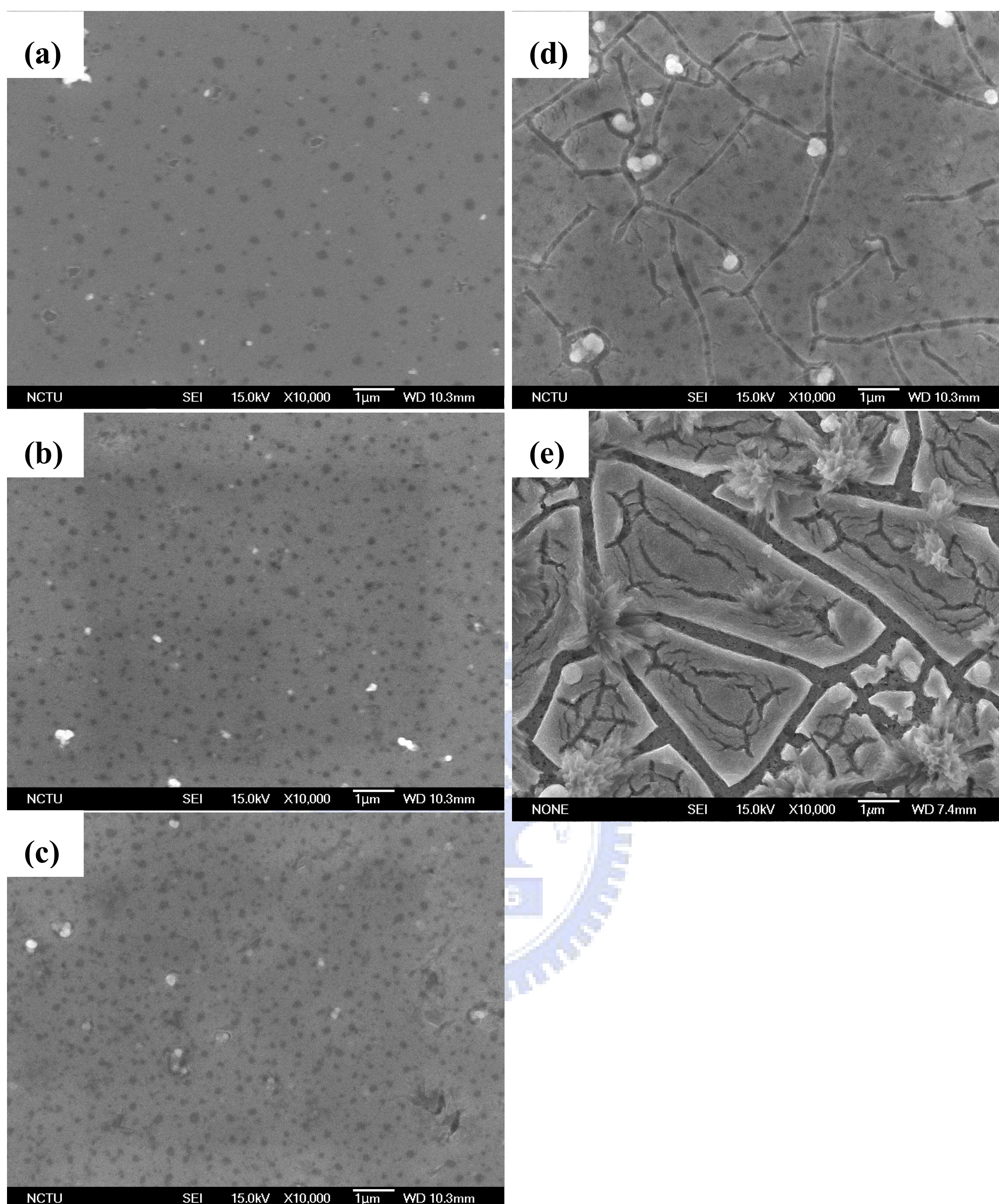

Figure 5.18 Planar views for the deposited films at various plating time with 0.06 M $NaNO_{2(aq)}$ after H_2 reduction at 200℃ for 2 hr; (a) 30, (b) 60, (c) 120, (d) 240, and (e) 480 min, respectively.

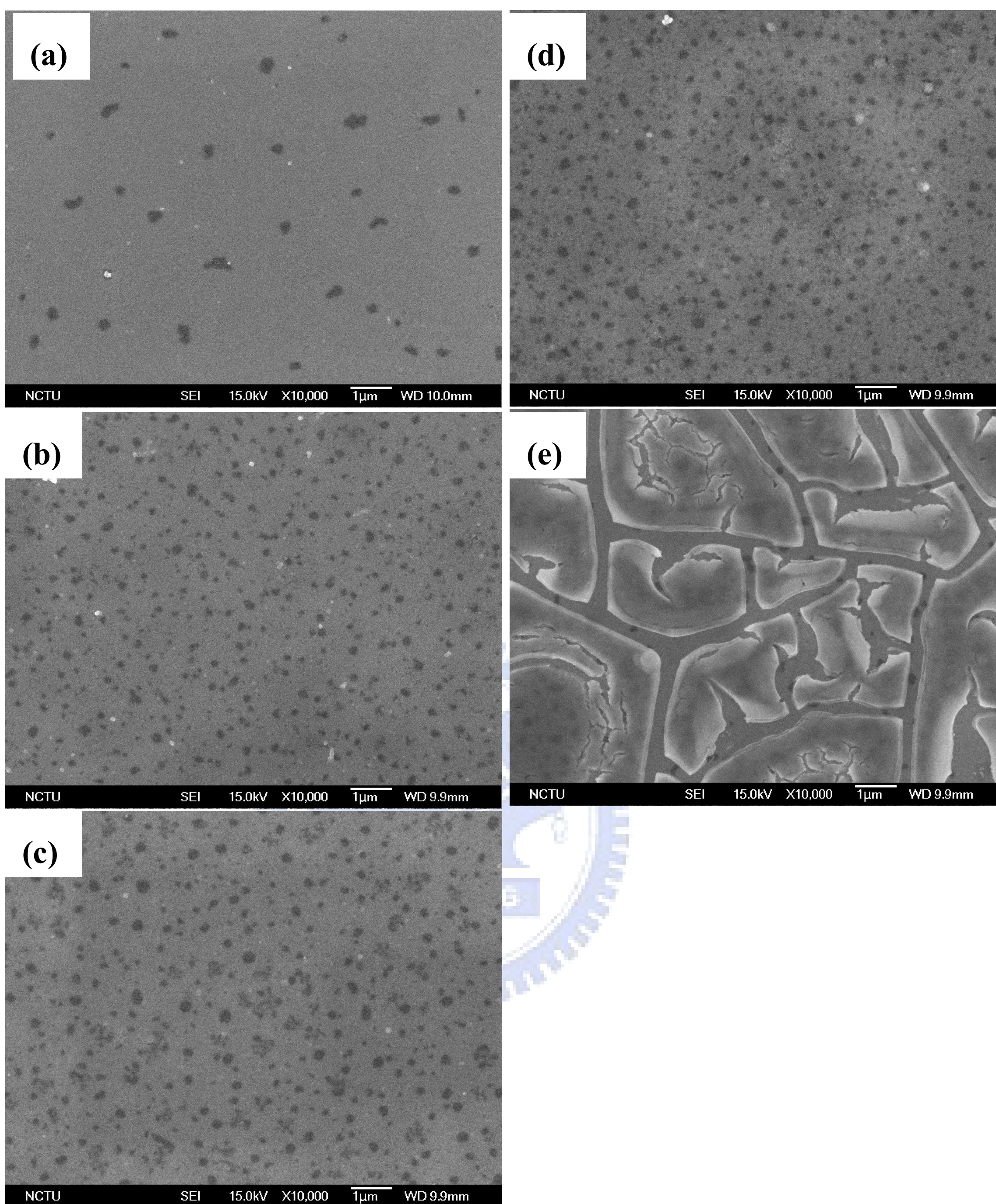

Figure 5.19 The planar views of deposited films at various plating time with 0.03 M $NaNO_{2(aq)}$ after H_2 reduction at 200℃ for 2 hr; (a) 30, (b) 60, (c) 120, (d) 240, and (e) 480 min, respectively.

5.2.2 Phase and crystallinity characterization for the deposited films after hydrogen reduction

Figure 5.20 displays the XRD analysis for the as-deposited films with various concentrations of $NaNO_{2(aq)}$ for 480 min plating time followed by H_2 reduction at 200 ℃ for 2 hr. In Figure 5.20, some diffraction peaks were observed, and they were assigned to ruthenium metal at 38° (100), 42° (002), 44° (101), respectively. On the other hand, no diffraction peaks for the ruthenium oxide were observed after hydrogen reduction. This result suggested that RuO_2 and Ru composite films were successfully reduced to ruthenium metal films by hydrogen. However, the widths for the diffraction peaks in Figure 5.20 were broad after hydrogen reduction. Therefore, we suspect that the films were crystallized with poor crystallinity by H_2 reduction at 200℃. That is to say, the amorphous as-deposited films were reduced to crystalline ruthenium metal films after hydrogen treatment.

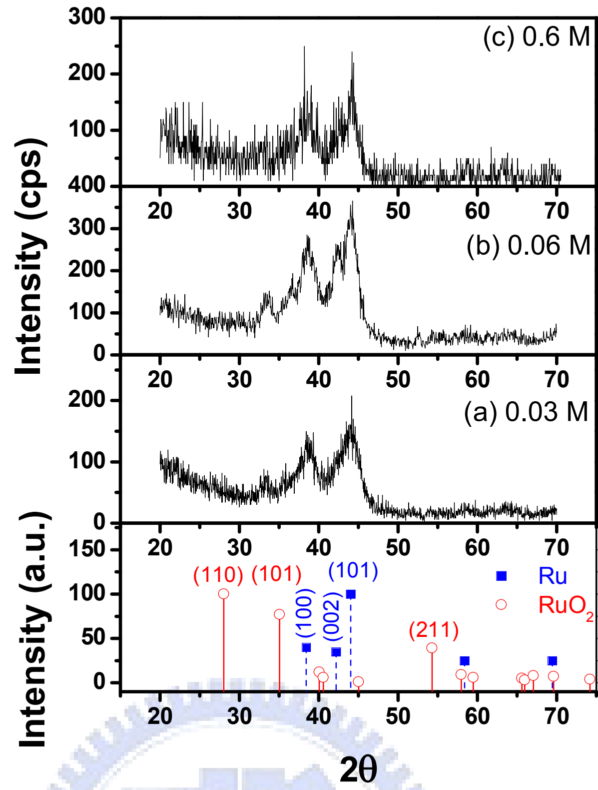

Figure 5.20 XRD patterns for the as-deposited films with various concentrations $NaNO_{2(aq)}$ for 480 min plating time and followed by H_2 reduction at 200℃ for 2 hr versus the standard pattern; (a) 0.03, (b) 0.06, and (c) 0.6 M, respectively.

5.2.3 Characterization of the oxidation states for the deposited films after hydrogen reduction

Figure 5.21 demonstrates the XPS spectra of Ru 3p3/2 line for the deposited film with 0.06 M $NaNO_{2(aq)}$ at 120 and 480 min plating time followed by H_2 reduction for 2 hr at 200℃. The binding energies of the deposited films in Figure 5.21 were 462.2 and 462.7 eV, respectively. In comparison to the results in Figure 5.8, the binding energies in Figure 5.21 shifted to lower energy, which suggested that the primary oxidation states of ruthenium decreased after hydrogen reduction. This result indicates that the composite films have been reduced to ruthenium metal films. In addition, this finding agreed well with the results of XRD in Figure 5.20 mentioned above.

Figure 5.22 presents the XPS spectra of oxygen 1s line for the deposited films described in Figure 5.21. The binding energies were 532 and 532.1 eV, respectively. Compared with the results in Figure 5.9, Figure 5.22 revealed absence of small shoulder at higher binding energy, from 535 to 540 eV. This result suggested that the ruthenium oxide in the composite films was successfully reduced to metallic ruthenium by hydrogen. In addition, the signal of oxygen in Figure 5.22 indicated that water was adsorbed on surface of the films.

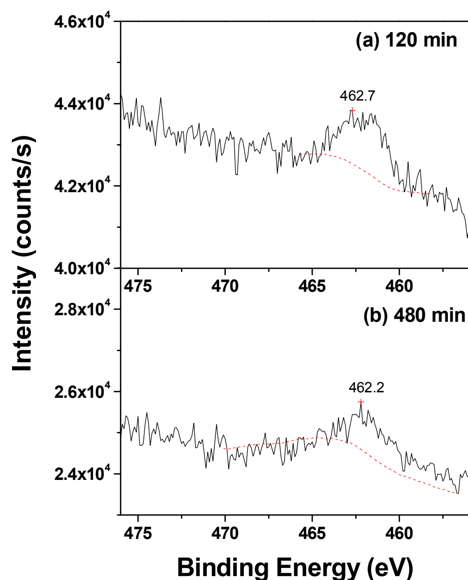

Figure 5.21 XPS spectra for the Ru 3p3/2 line from the deposited films with 0.06 M $NaNO_{2(aq)}$ at various plating time followed by H_2 reduction at 200℃ for 2 hr; (a) 120 and (b) 480 min, respectively.

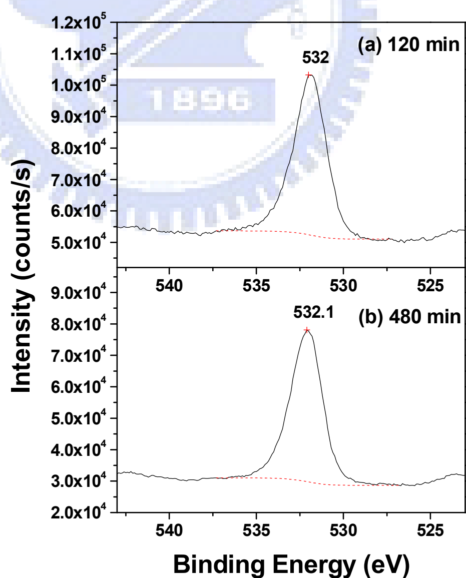

Figure 5.22 XPS spectra for the O 1s line from the deposited films with 0.06 M $NaNO_{2(aq)}$ at various plating time followed by H_2 reduction at 200℃ for 2 hr; (a) 120 and (b) 480 min, respectively.

5.2.4 Raman spectroscopy characterization for the deposited films after hydrogen reduction

Raman spectra for the composite films with 0.6 M $NaNO_{2(aq)}$ at various plating time followed by hydrogen reduction are shown in Figure 5.23. In comparison to the results of Figure 5.14, no stretching modes of RuO_2 and broad peaks were observed. This result indicated that ruthenium oxides in the composite films were completely reduced to ruthenium metal by hydrogen. On the other hand, no broad peak at 500 cm^{-1} suggested that strain caused by lattice mismatch was decreased considerably. That ruthenium oxide was reduced to ruthenium, which would lead to the volume reduction, produced more defects in the deposited films so that the strain was decreased.

Figure 5.24 and Figure 5.25 exhibit Raman spectra for the composite films at various plating time with 0.06 and 0.03 M $NaNO_{2(aq)}$ followed by hydrogen reduction. Similarly, the results mentioned in Figure 5.23 were observed in Figure 5.24 and Figure 5.25 as well.

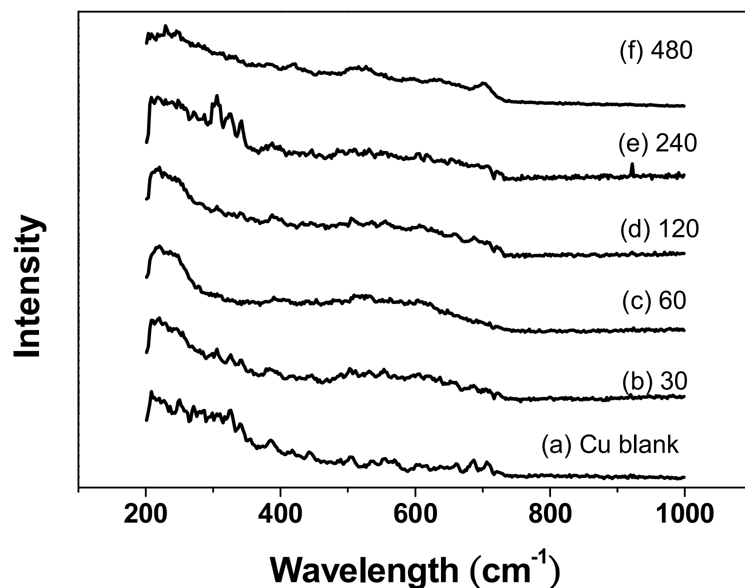

Figure 5.23 Raman spectra for the composite films with 0.6 M $NaNO_{2(aq)}$ at various plating times after H_2 reduction; (a) Cu substrate as a blank, (b) 30, (c) 60, (d) 120, (e) 240, and (f) 480 min, respectively.

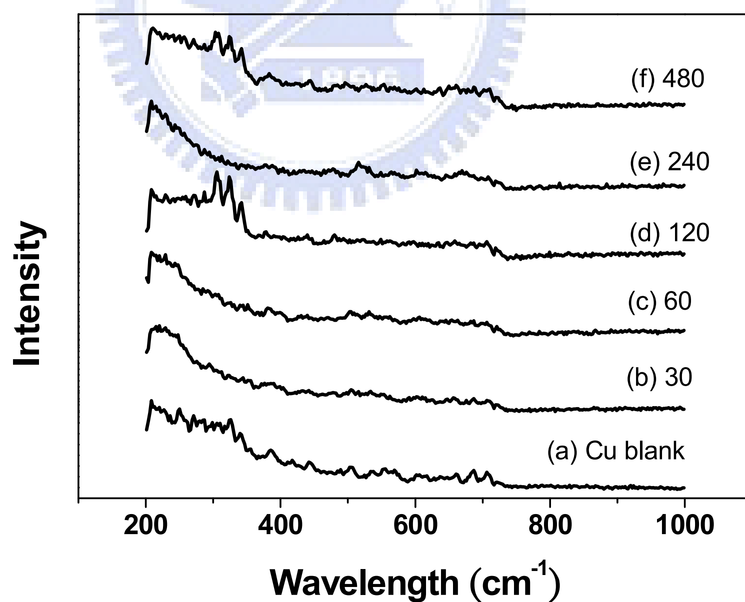

Figure 5.24 Raman spectra for the composite films with 0.06 M $NaNO_{2(aq)}$ at various plating times after H_2 reduction; (a) Cu substrate as a blank, (b) 30, (c) 60 , (d) 120, (e) 240, and (f) 480 min, respectively.

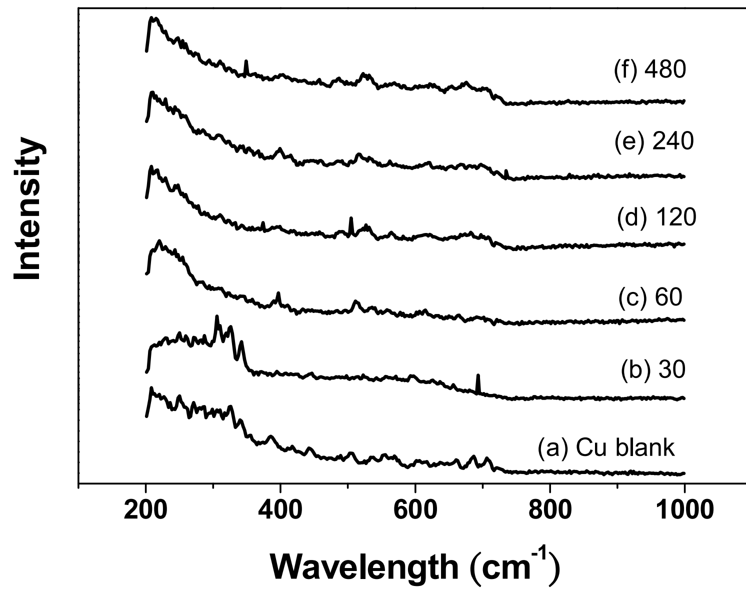

Figure 5.25 Raman spectra for the composite films with 0.03 M $NaNO_{2(aq)}$ at various plating times after H_2 reduction; (a) Cu substrate as a blank, (b) 30, (c) 60, (d) 120, (e) 240, and (f) 480 min, respectively.

5.3 Characterization of composite RuO_2 and Ru films after argon annealing

5.3.1 Morphology observation of the deposited films after argon annealing

Figure 5.26 displays the planar views of SEM images for the composite films at 30, 120, and 480 min plating time with 0.06 M $NaNO_{2(aq)}$ followed by Ar annealing for 2 hr at 400℃. In Figure 5.26, the composite films remained smooth with small particles after Ar annealing. In comparison to the results in Figure 5.3, the particles in the composite films in Figure 5.26 became larger after argon annealing. The behavior resulted from diffusion of materials at elevated temperature. The components for the deposited films, RuO_2 and Ru, were likely to aggregate at 400℃. Therefore, the particle sizes for the composite films in Figure 5.26 were increased compared with that in Figure 5.3.

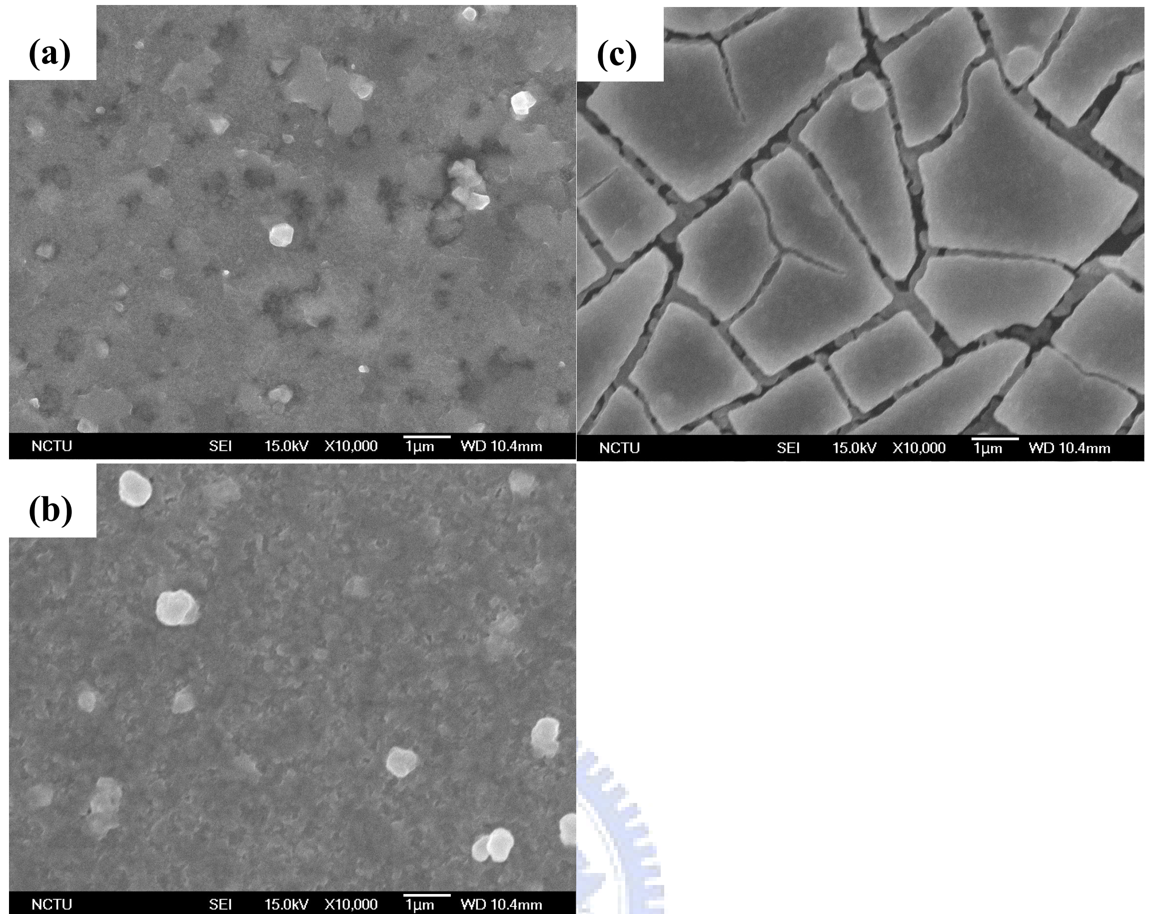

Figure 5.26 Planar views for the deposited films at various plating time with 0.06 M $NaNO_{2(aq)}$ followed by Ar annealing at 400℃ for 2 hr; (a) 30, (b) 120, and (c) 480 min, respectively.

5.3.2 Phase and crystallinity characterization for the deposited films after argon annealing

Figure 5.27 provides the as-deposited films with different concentrations of $NaNO_{2(aq)}$ for 480 min plating time followed by argon annealing at 400℃ for 2 hr. Because the XRD analysis in Figure 5.13 suggested that the as-deposited films were amorphous, the as-deposited films underwent argon annealing to crystallize the amorphous films. Annealing was performed under Ar atmosphere because ruthenium was easily oxidized by oxygen under elevated temperature [19]. In Figure 5.27, in addition to the diffraction peaks from substrate, both diffraction peaks of ruthenium oxide and that of ruthenium were observed. This result indicated that the as-deposited amorphous films became crystalline composite films. In addition, this finding is compatible with the result of XPS in Table 5.2.

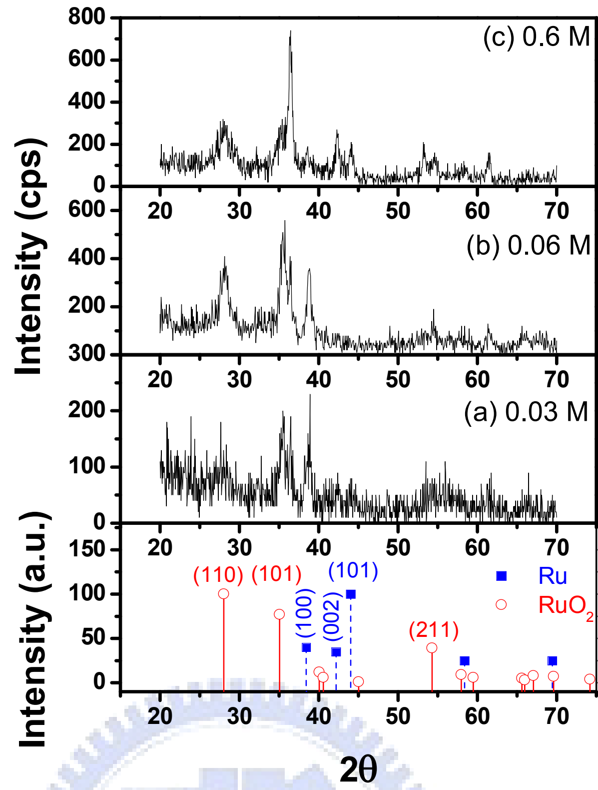

Figure 5.27 XRD patterns for the as-deposited films with various concentrations $NaNO_{2(aq)}$ for 480 min plating time followed by Ar annealing at 400℃ for 2 hr versus the standard pattern; (a) 0.03, (b) 0.06, and (c) 0.6 M, respectively.

Chapter 6 Conclusions

We summarize the significant finding in following points;

1. A novel electroless plating recipe was developed to deposit composite RuO_2 and Ru composite films. Its formulation included $K_2RuCl_5 \cdot xH_2O$, $NaNO_2$, NaOH, and NaClO.

2. Different adding steps, three concentrations of $NaNO_2$, and various plating time were selected during the deposition process. In addition, a two-stage electroless reaction step is presented with clear explanation.

3. Stability for the plating solutions was confirmed by UV-Vis absorption spectra with narrow maximum wavelength distribution. Lifetime for the plating baths with different concentrations of $NaNO_{2(aq)}$ at 40℃ was determined from 36–160 hr. In contrast, at room temperature the lifetime was 132–209 hr. Besides, the results of XPS for the deposited films with various plating time suggest that the components during the entire plating process remain the same.

4. From a variety of qualitative characterization, the as-deposited film was identified as an amorphous RuO_2 and Ru composite film. Its thickness ranged from 35–300 nm, and the uniformity from 120 min plating time was between 2.05–6.70%.

5. Combining results of plating solution lifetime and that of roughness for the as-deposited films, the desirable concentration for the $NaNO_2$ was 0.06 M.

6. A crystalline Ru film was demonstrated by a H_2 annealing on the composite film at 200℃ for 2 hr.

7. A crystalline RuO_2 and Ru composite film was obtained via carrying out the an Ar annealing at 400℃ for 2 hr on the composite film.

References

[1] Spendelow JS, Wieckowski A. Noble metal decoration of single crystal platinum surfaces to create well-defined bimetallic electrocatalysts. Physical Chemistry Chemical Physics. 2004;6(22):5094-118.

[2] Oh SH, Park CG, Park C. Thermal stability of RuO_2/Ru bilayer thin film in oxygen atmosphere. Thin Solid Films. 2000;359(1):118-23.

[3] Josell D, Wheeler D, Witt C, Moffat TP. Seedless superfill: Copper electrodeposition in trenches with ruthenium barriers. Electrochem Solid State Lett. 2003;6(10):C143-C5.

[4] Cho SK, Kim SK, Han H, Kim JJ, Oh SM. Damascene Cu electrodeposition on metal organic chemical vapor deposition-grown Ru thin film barrier. Journal of Vacuum Science & Technology B. 2004;22(6):2649-53.

[5] Kang SY, Hwang CS, Kim HJ. Improvements in growth behavior of CVD Ru films on film substrates for memory capacitor integration. Journal of the Electrochemical Society. 2005;152(1):C15-C9.

[6] Ogawa S, Tarumi N, Abe M, Shiohara M, Imamura H, Kondo S, et al. Amorphous Ru/polycrystalline Ru highly reliable stacked layer barrier technology. IEEE International Intercconnect Technology Conference; 2008; Burlingame, CA; 2008. p. 102-4.

[7] Hu CC, Huang YH. Cyclic voltammetric deposition of hydrous ruthenium oxide for electrochemical capacitors. Journal of the Electrochemical Society. 1999;146(7):2465-71.

[8] Fang QL, Evans DA, Roberson SL, Zheng JP. Ruthenium oxide film electrodes prepared at low temperatures for electrochemical capacitors. Journal of the Electrochemical Society. 2001;148(8):A833-A7.

[9] Rarnani M, Haran BS, White RE, Popov BN. Synthesis and characterization of hydrous ruthenium oxide-carbon supercapacitors. Journal of the Electrochemical Society. 2001;148(4):A374-A80.

[10] Chang KH, Hu CC. Oxidative synthesis of $RuO_x \cdot nH_2O$ with ideal capacitive characteristics for supercapacitors. Journal of the Electrochemical Society. 2004;151(7):A958-A64.

[11] Kim IH, Kim KB. Ruthenium oxide thin film electrodes prepared by electrostatic spray deposition and their charge storage mechanism. Journal of the Electrochemical Society. 2004;151(1):E7-E13.

[12] Kim IH, Kim JH, Lee YH, Kim KB. Synthesis and characterization of electrochemically prepared ruthenium oxide on carbon nanotube film substrate

for supercapacitor applications. Journal of the Electrochemical Society. 2005;152(11):A2170-A8.

[13] Hu CC, Liu MJ, Chang KH. Anodic deposition of hydrous ruthenium oxide for supercapacitors. Journal of Power Sources. 2007;163(2):1126-31.

[14] Kim JH, Kil DS, Yeom SJ, Roh JS, Kwak NJ, Kim JW. Modified atomic layer deposition of RuO_2 thin films for capacitor electrodes. Applied Physics Letters. 2007;91(5).

[15] Glenn O. Mallory, Hajdu JB, eds. Electroless plating : fundamentals and applications Orlando, Fla: American Electroplaters and Surface Finishers Society 1990.

[16] Okuno K. Application of electroless ruthenium deposits for elecronic materials. Plat Surf Finish. 1990;77(2):48-52.

[17] Chang YS, Chou ML. Microstructure evolution of newly developed electroless ruthenium deposition on silicon observed by scanning by transmission electron microscope. J Appl Phys. 1991;69(11):7848-52.

[18] Lysczek EM, Mohney SE. Selective deposition of ohmic contacts to p-InGaAs by electroless plating. Journal of the Electrochemical Society. 2008;155(10):H699-H702.

[19] Sergio Trasatti, O'Grady WE. Advances in electrochemistry and electrochemical engineering. New York: Wiley 1982:177-261.

[20] Kroschwitz JI. Kirk-Othmer encyclopedia of chemical technology. Hoboken, N.J.: Wiley-Interscience 2004.

[21] Lee JG, Kim YT, Min SK, Choh SH. Effects of excess oxygen on the properties of reactivity sputtered RuO_x thin-films. J Appl Phys. 1995;77(10):5473-5.

[22] Si J, Desu SB. RuO_2 films by metal-organic chemical vapor deposition. Journal of Materials Research. 1993;8(10):2644-8.

[23] Yuan Z, Puddephatt RJ, Sayer M. Low-temperature chemical vapor deposition of ruthenoum dioxide from ruthenium tertoxide: a simple approach to high-purity RuO_2 films. Chem Mat. 1993;5(7):908-10.

[24] Hashaikeh R, Butler IS, Kozinski JA. Thin-film ruthenium dioxide coatings via ozone-mediated chemical vapor deposition. Thin Solid Films. 2006;515(4):1918-21.

[25] Rochefort D, Dabo P, Guay D, Sherwood PMA. XPS investigations of thermally prepared RuO_2 electrodes in reductive conditions. Electrochim Acta. 2003;48(28):4245-52.

[26] Kawano K, Nagai A, Kosuge H, Shibutami T, Oshima N, Funakubo H. Seed layer free conformal ruthenium film deposition on hole substrates by MOCVD using (2,4-dimethylpentadienyl)(ethylcyclopentadienyl)ruthenium. Electrochem

Solid State Lett. 2006;9(7):C107-C9.

[27] Kim SK, Lee SY, Lee SW, Hwang GW, Hwang CS, Lee JW, et al. Atomic layer deposition of Ru thin films using 2,4-(dimethylpentadienyl)(ethylcyclopentadienyl)Ru by a liquid injection system. Journal of the Electrochemical Society. 2007;154(2):D95-D101.

[28] Arunagiri TN, Zhang Y, Chyan O, El-Bouanani M, Kim MJ, Chen KH, et al. 5 nm ruthenium thin film as a directly plateable copper diffusion barrier. Applied Physics Letters. 2005;86(8):3.

[29] Jia Z, Ren TL, Liu TZ, Hu H, Zhang ZG, Xie D, et al. Study on oxidization of Ru and its application as electrode of PZT capacitor for FeRAM. Materials Science and Engineering B-Solid State Materials for Advanced Technology. 2007 Apr;138(3):219-23.

[30] Shin JH, Waheed A, Winkenwerder WA, Kim HW, Agapiou K, Jones RA, et al. Chemical vapor deposition of amorphous ruthenium-phosphorus alloy films. Thin Solid Films. 2007;515(13):5298-307.

[31] Heo JY, Lee SY, Eom D, Hwang CS, Kim HJ. Enhanced nucleation Behavior of atomic-layer-deposited ru film on low-k dielectrics afforded by UV-O_3 treatment. Electrochem Solid State Lett. 2008;11(2):G5-G8.

[32] Aaltonen T, Alen P, Ritala M, Leskela M. Ruthenium thin films grown by atomic layer deposition. Chem Vapor Depos. 2003;9(1):45-9.

[33] Chan HYH, Takoudis CC, Weaver MJ. High-pressure oxidation of ruthenium as probed by surface-enhanced Raman and X-ray photoelectron spectroscopies. J Catal. 1997;172(2):336-45.

[34] Kim YS, Kim HI, Dar MA, Seo HK, Kim GS, Ansari SG, et al. Electrochemically deposited ruthenium seed layer followed by copper electrochemical plating. Electrochem Solid State Lett. 2006;9(1):C19-C23.

[35] Kim YS, Kim HI, Cho JH, Seo HK, Kim GS, Ansari SG, et al. Electrochemical deposition of copper and ruthenium on titanium. Electrochim Acta. 2006;51(25):5445-51.

[36] Thambidurai C, Kim YG, Stickney JL. Electrodeposition of Ru by atomic layer deposition (ALD). Electrochim Acta. 2008;53(21):6157-64.

[37] Wolfe S, Hasan SK, Campbell JR. Ruthenoum trichloride-catalysed hopochlirode oxidation of organic compounds. Journal of the chemical societyD, Chemical communications. 1970:1420-1.

[38] Seddon EA. The Chemistry of Ruthenium. Amsterdam ; New York: Elsevier 1984.

[39] 呂咏錚. 無電鍍金屬釕及其應用於銅擴散阻障層之研究: 國立交通大學; 2008.

[40] Pagliaro M, Campestrini S, Ciriminna R. Ru-based oxidation catalysis. Chemical Society Reviews. 2005;34(10):837-45.

[41] Sayama K, Abe R, Arakawa H, Sugihara H. Decomposition of water into H_2 and O_2 by a two-step photoexcitation reaction over a Pt-TiO_2 photocatalyst in $NaNO_2$ and Na_2CO_3 aqueous solution. Catalysis Communications. 2006;7(2):96-9.

[42] Mar SY, Chen CS, Huang YS, Tiong KK. Characterization of RuO_2 thin films by Raman spectroscopy. Appl Surf Sci. 1995;90(4):497-504.